Table Of Contents

I. FISCHER-TROPSCH SYNTHESIS ON IRON CATALYSTS

1. Background

1.1. Structure and Function of Active Phases in Fischer-Tropsch Synthesis

Fe-based oxides have been used as commercial catalysts for Fischer-Tropsch synthesis (FTS) to produce a wide range of paraffin and olefin products, ranging from methane to high molecular weight waxes [1]. During activation in synthesis gas and subsequent FTS reactions, several phases including metallic iron, iron carbides and iron oxides can co-exist at steady-state conditions [2-5]. The relative amounts of these phases depend on various activation and reaction conditions, which also lead to different catalytic performance. Some researchers [6] have proposed that surface iron atoms are responsible for FTS activity, while others have considered surface carbides or a mixture of carbides [7,8] with metallic iron [9] to be the active phase. There are also some reports that suggest that magnetite Fe_3O_4 is the active FTS phase [10-12]. Although these studies have each provided some evidence to support its specific proposal about the active phase, the available information remains phenomenological and sometimes contradictory, and a direct method to identify the active phase during reaction and to count the number of active sites has remained elusive. Our previous studies of the active phases and catalytic activity of Fe-Zn-K-Cu oxides [18-27], address the structure and site requirement for Fe-based FTS catalysts. During this reporting period, we present a manuscript that summarizes the effects of the different promoters, Zn, K and Cu on the reduction/carburization of Fe oxides and their catalytic behavior.

1.2. Effects of Zn, Ru (Cu) and K on Fe Oxides

Many components have been incorporated into Fe catalysts in order to improve their mechanical and catalytic properties. Our previous studies have shown that Zn, K and Cu [13-15] promote the catalytic properties of Fe oxides. Zinc oxide, as a non-reducible oxide at FTS conditions, appears to stabilize the surface area of Fe oxide precursors. Alkali, as a modifier of the adsorption enthalpies of H_2 and CO, has been reported to increase the selectivity to desired C_{5+} products. Copper promotes the carburization processes and decreases the temperature required for the activation of iron oxide precursors. In this report, we discuss in detail the individual effects of each of these promoters on the reduction/carburization, structure and performance of Fe catalysts for the FTS reactions.

2. Synthesis Procedures

2.1 Fe-Zn-K-Cu Oxides

Fe-Zn-K-Cu catalysts were prepared by co-precipitation of iron and zinc nitrates followed by subsequent impregnation of aqueous solutions of $K_2(CO_3)$ and $Cu(NO_3)_2$ using the procedure described in our previous report [18]. Then, the dried materials were treated in dry air at 673 K for 4 h. The K/Fe ratio was varied from 0 to 0.04, Zn/Fe from 0 to 0.4 and Cu/Fe ratio from 0 to 0.02.

3. Catalyst Characterization

3.1. Protocols for the Characterization of Fe-based FTS Catalysts

This research program addresses the synthesis and the structural and catalytic characterization of active sites in Fe-based catalysts for FTS. We have designed a matrix of samples consisting of a systematic range of multi-component catalysts in order to determine the number and type of surface sites present on fresh catalysts and on samples during and after FTS reaction (Table 1.1). Our objective is to develop rigorous relationships between the promoters, the resulting catalyst structures, and their function in FTS reactions.

4. Structures and Site Requirement of Fe-Zn-K-Cu Oxides for Fischer-Tropsch Synthesis

The reduction, carburization, and catalytic properties of Fe-Zn-K-Cu oxide catalysts were examined using kinetic and spectroscopic methods at FTS conditions. The structure and site requirements for FTS reactions and the effect of Zn, K and Cu were discussed in the following manuscript.

Table 1.1. Matrix of samples and characterization methods for FTS reaction

<table>
<tr><th colspan="3">Nominal Composition of the Catalysts</th><th rowspan="2">Characterization Before and After FTS</th><th rowspan="2">FTS reaction</th></tr>
<tr><th>Zn/Fe mole ratio</th><th>K/(Fe+Zn) (at.%)</th><th>Cu/(Fe+Zn) (at.%)</th></tr>
<tr><td rowspan="6">0</td><td rowspan="2">0</td><td>0</td><td rowspan="24">XRD

Surface area

In-situ
XAS

H_2-TPR

CO-TPR</td><td rowspan="24">Effect of reaction condition

220 ^oC
21.4 atm

235 ^oC
21.4 atm

270 ^oC
5 atm

Effect of CO_2 addition

Isotopic studies</td></tr>
<tr><td>1</td></tr>
<tr><td rowspan="3">2</td><td>0</td></tr>
<tr><td>1</td></tr>
<tr><td>2</td></tr>
<tr><td>4</td><td>1</td></tr>
<tr><td rowspan="3">0.05</td><td>0</td><td>0</td></tr>
<tr><td>2</td><td>1</td></tr>
<tr><td>4</td><td>2</td></tr>
<tr><td rowspan="6">0.1</td><td rowspan="2">0</td><td>0</td></tr>
<tr><td>1</td></tr>
<tr><td rowspan="3">2</td><td>0</td></tr>
<tr><td>1</td></tr>
<tr><td>2</td></tr>
<tr><td>4</td><td>1</td></tr>
<tr><td rowspan="3">0.2</td><td>0</td><td>0</td></tr>
<tr><td>2</td><td>1</td></tr>
<tr><td>4</td><td>2</td></tr>
<tr><td rowspan="6">0.4</td><td rowspan="2">0</td><td>0</td></tr>
<tr><td>1</td></tr>
<tr><td rowspan="3">2</td><td>0</td></tr>
<tr><td>1</td></tr>
<tr><td>2</td></tr>
<tr><td>6</td><td>1</td></tr>
</table>

4.1. Effects of Zn, Cu and K Promoters on the Structure, Reduction/Carburization Behavior, and Performance of Fe-based Fischer-Tropsch Synthesis Catalysts

Abstract

Zn, K and Cu effects on the structure and surface area, and on the reduction, carburization, and catalytic behavior of Fe-Zn and Fe oxides used as precursors to Fischer-Tropsch synthesis (FTS) catalysts precursors were examined using X-ray diffraction, kinetic studies of the reactions of H_2 or CO with Fe-Zn oxides promoted with K and Cu, and FTS reaction rate measurements. Fe_2O_3 precursors initially reduce to reduce to Fe_3O_4 and then to metallic Fe (in H_2) or to a mixture of $Fe_{2.5}C$ and Fe_3C (in CO). Zn, present as $ZnFe_2O_4$, increases the surface area of precipitated oxide precursors by inhibiting sintering during thermal treatment and during activation in H_2/CO reactant mixtures, leading to higher FTS rates than on ZnO-free precursors. $ZnFe_2O_4$ species do not reduce to active FTS catalysts and instead lead to the loss of active components; as a result, maximum FTS rates are achieved at intermediate Zn/Fe contents. Cu increases the rate of Fe_2O_3 reduction to Fe_3O_4 by providing H_2 dissociation sites. Potassium increases CO activation rates and increases the rate of carburization of Fe_3O_4. In this manner, Cu and K promote the nucleation of oxygen-deficient FeO_x species involved in reduction and carburization and decrease the ultimate size of the Fe oxide and carbide structures formed during activation in synthesis gas. As a result, Cu and K increase FTS rates on catalysts formed from Fe-Zn oxide precursors. Cu increases CH_4 and the paraffin content of FTS products, but the additional presence of K inhibits these effects. Potassium titrates residual acid and hydrogenation sites and increases the olefin content and molecular weight of FTS products. K increases the rate of secondary water gas shift reactions, while Cu increases the relative rate of oxygen removal as CO_2 instead of water. Through these two different mechanisms, K and Cu both increase the CO_2 selectivity on FTS catalysts prepared from Fe-Zn oxide precursors.

Introduction

Iron oxides are precursors for Fischer-Tropsch synthesis (FTS) catalysts, which convert synthesis gas (H_2/CO) to useful chemicals and liquid hydrocarbons [1-4]. These oxides transform into active structures during initial contact with synthesis gas at typical reaction temperatures. Several Fe phases, such as Fe metal, Fe carbides (FeC_x) or oxides (FeO_x) form and have been proposed to act as active structures during steady-state Fischer-Tropsch synthesis [5-12]. Oxides (ZnO, MnO, Al_2O_3), metals (Cu, Ru), and alkali (K, Na, Cs, Rb) oxides or carbonates are typically added to Fe oxide precursors as promoters in order to improve their structural integrity or catalytic properties. For example, ZnO, Cu, and K compounds have been reported to increase FTS rates on precipitated Fe_2O_3 precursors [13-17]. Some earlier studies have suggested that K promotes CO chemisorption and inhibit hydrogen chemisorption, which in turn results in lower FTS rates, higher molecular weight and greater olefin content [3,14], although it is unclear how the prevalent K_2CO_3 and FeC_x interact in order to produce the atomic contact required for the proposed electronic effects. Cu, when present along with K increases FTS rates without detectable changes in selectivity [17,18]. Cu and K compounds have also been reported to increase the activity for water gas shift (WGS) [14,16], a reaction that occurs concurrently with FTS on many Fe-based catalysts. Our previous studies have shown that Cu or Ru oxides in intimate mixtures with a Fe-Zn-K precursor matrix increases the rate of reduction the reduction and carburization of the Fe oxide component in these precursors, which in turn leads to the formation of smaller FeC_x crystallites, to greater active site densities, and to higher FTS rates [17,19,20]. Hence Cu and Ru do not serve as chemical promoters on K-promoted catalysts, but instead provide a better dispersion of the active phase and a greater availability of active sites.

We examine here a series of co-precipitated Fe and Zn oxides containing Zn, Cu and K (Zn/Fe=0-0.4, K/Fe=0-0.04, Cu/Fe=0-0.02; atomic ratios) in order to probe the roles of these additives on the structure, reduction/carburization behavior, and catalytic properties of Fe oxides. The surface area, bulk structure, and reduction and carburization behavior were systematically investigated using BET surface area measurements, X-ray diffraction (XRD) and temperature-programmed reaction (TPR) studies. In parallel, steady-state FTS rates and selectivities were measured as a function of the Zn, K and Cu contents at typical FTS conditions (493 K, 3.16 MPa) using a tubular reactor with plug-flow hydrodynamics in order to relate the observed catalytic promotion to the active structures formed during activation of the oxide precursors in H_2/CO mixtures.

Experimental

Synthesis of Fe_2O_3-Zn-K-Cu catalysts

Fe_2O_3-Zn-K-Cu catalysts were prepared by co-precipitation of Fe and Zn nitrates at a constant pH to form porous Fe-Zn oxyhydroxide powders, which were promoted after treatment in air by impregnation of K_2CO_3 and $Cu(NO_3)_2$. A mixture solution containing both $Fe(NO_3)_3$ (Aldrich, 99.9+%, 3.0 M) and $Zn(NO_3)_2$ (Aldrich, 99.9+%, 1.4 M) with varying atomic ratios (0-0.4) and a separate solution of $(NH_4)_2CO_3$ (Aldrich, 99.9%, 1 M) were used in the precipitation procedure. The Zn/Fe solution was added (120 cm^3/h) into a flask containing deionized water (~ 50 cm^3) at 353 K using a liquid pump. $(NH_4)_2CO_3$ was added simultaneously and its rate was controlled in order to keep the pH of the slurry at 7.0±0.1 (Omega, PHB-62 pH Meter). The precipitated powders (~ 20 g) were washed five times with doubly distilled deionized water (~ 1000 cm^3/g each time), and dried in ambient air at 393 K overnight. The dried precursors were finally treated in flowing dry air at 623 K for 1 h.

Promoters were added to these precursors by impregnation with aqueous solutions of K_2CO_3 (Aldrich, 99.99%, 0.16 M) and/or $Cu(NO_3)_2$ (Aldrich, 99.99%, 0.16 M) to give the desired K/Fe and Cu/Fe atomic ratios. The impregnated samples were dried at 393 K in ambient air and then treated in flowing dry air at 673 K for 4 h, a procedure that led to the complete decomposition of all precursor salts except K_2CO_3 [21]. The resulting powders consisted of CuO, ZnO, Fe_2O_3 and K_2CO_3, as shown by a combination of chemical analysis, identification of decomposition products, X-ray diffraction, and X-ray absorption spectroscopy.
These samples are denoted as Fe_2O_3-Zn-Cu_x, Fe_2O_3-Zn-K_y, or Fe_2O_3-Zn-K_y-Cu_x, throughout, where x and y represent the atomic ratios of the respective elements relative to Fe in each sample. All samples were pressed into pellets (443 MPa), crushed, and sieved to retain 100-180 μ particles that were used in all experiments.

Catalyst Characterization

Powder X-ray diffraction (XRD) measurements were carried out using a Siemens Diffractometer D-5000 and Cu Kα radiation (λ = 1.5406 Å). BET surface areas were measured using an Autosorb 6 automated system (Quantachrome, Inc.) and using N_2 physisorption at its normal boiling point, after evacuating the samples at 393 K for 3 h.

The rates of reduction and carburization of K- and/or Cu-promoted Fe_2O_3-Zn were measured by using temperature-programmed reaction (TPR) methods with H_2 or CO as the reactant. Samples (0.2 g) were placed in a quartz cell (10 mm i.d.) and first treated in 20% O_2 in Ar (0.268 mol/h) to 673 K at 0.33 K/s, held at 673 K for 900 s, and then cooled to ambient temperature in Ar. The flow was then switched to 20% H_2 or 20% CO in Ar (0.268 mol/h) and the reactor temperature was increased to 1000 K at 0.167 K/s. The concentration of reactants and products were measured using a mass spectrometer (Leybold Inficon Instruments Co., Inc.) equipped with a differentially pumped sampling system.

Fischer-Tropsch Synthesis Rates and Selectivities

Steady-state FTS reaction rates and selectivities were measured in a single-pass fixed bed reactor (SS 304, 1.27 cm o.d. and 1 cm i.d., enclosed by a three-zone furnace equipped with temperature controllers (Watlow Series 982 and 988). The actual temperature of the catalyst was monitored axially using a type-K movable thermocouple; it was within ±0.5 K of the average bed temperatures throughout the reactor length. All lines after the outlet of the reactor were kept at 433-553 K. The reactor system also included two stainless steel 75 cm^3 traps. A hot trap at 408 K and reactor pressure was placed immediately below the reactor to collect heavy hydrocarbon products. A trap at ambient temperature and pressure was placed after the chromatograph sampling valve and used to collect water, oxygenates, and light hydrocarbons.

Synthesis gas (Praxair, 62% H_2, 31% CO and 7% N_2, N_2 internal standard) was first purified by removing metal carbonyls (activated charcoal trap, Sorb-Tech RL-13) and water (molecular sieve trap, Matheson, Model 452A). Synthesis gas flow was controlled using an electronic mass-flow controller (Porter, Model 201-AFASVCAA). Catalyst samples (0.4 g, 100-180 μ) diluted with quartz granules (11 g, 100-180 μ) were activated in synthesis gas at 0.1 MPa by increasing the temperature from 298 K to 423 K at 0.167 K/s and then from 423 K to 543 K at 0.017 K/s. The samples were kept at 543 K for 1 h, before establishing FTS reaction conditions (493 K and 3.16 MPa). Product and reactant analysis was performed by gas chromatography (Hewlett Packard, Model 5890 Series II) using a 10-port sampling valve. The analysis of N_2, CO, CO_2, and light hydrocarbons was performed using a thermal conductivity detector and a Porapak Q packed column (15.2 cm × 0.318 cm). All hydrocarbons up to C_{15} were analyzed using a flame ionization detector and a cross-linked methyl silicone capillary column (HP-1, 50 m × 0.32 mm; 1.05 μ film).

Results and Discussion

Crystalline Structures in Fe_2O_3-Zn Precursors

X-ray powder diffraction patterns of Fe_2O_3-Zn precursors with Zn/Fe atomic ratios of 0-0.4 are shown in Figure 1. These diffraction data indicate that rhombohedral hematite (Fe_2O_3) with a corundum-type structure, forms in samples with Zn/Fe < 0.2, while a $ZnFe_2O_4$ phase with a cubic franklinite spinel-type structure appears along with hematite at higher Zn/Fe ratios. Fe_2O_3 and $ZnFe_2O_4$ co-exist at intermediate Fe/Zn ratios. $ZnFe_2O_4$ is the only detectable phase in the sample with the highest Zn/Fe ratio (0.4); its broad diffraction peaks reflect the Zn-deficient nature of the Fe-Zn spinel structure, which requires a Zn/Fe ratio of 0.5 for the stoichiometric $ZnFe_2O_4$ structure. Precipitated Fe-Zn oxides appear to be present in the form of a mixture of Fe_2O_3 and $ZnFe_2O_4$. The only Zn-containing phase is $ZnFe_2O_4$, and it acts as a textural promoter that increases the surface area of Fe_2O_3-Zn precursors, as shown in the next section. At low Zn concentrations (Figure 1; patterns a-c), Zn is detected only as small $ZnFe_2O_4$ crystallites, which appear to inhibit the sintering of Fe_2O_3 at high temperatures (623-673 K). At higher Zn contents (Figure 1; patterns d and e), it is likely that $ZnFe_2O_4$ crystallites provide a matrix for the isolation of individual Fe_2O_3 crystallites. Zn also titrates Fe by forming $ZnFe_2O_4$, a less reducible compound than Fe_2O_3; this tends to weaken the structural promotion by Zn by preventing the reduction of some of the Fe and its contribution to the active site manifold. Thus, intermediate Zn/Fe ratios are likely to lead to optimum catalytic performance. The impregnation of potassium and copper and the subsequent treatment in air did not influence the Fe-Zn oxide crystalline phases detected by X-ray diffraction. This shows that Fe-Zn oxide structures, once formed, remain stable during subsequent aqueous impregnation and thermal treatment.

Surface Areas of Fe_2O_3-Zn-K-Cu Oxide Precursors

The textural promotion effects of $ZnFe_2O_4$ on the surface area of Fe oxide precursors were examined by N_2 physisorption measurements of K- and/or Cu-promoted Fe_2O_3-Zn samples. The BET surface area of Fe_2O_3-Zn-K-Cu increased monotonically with increasing Zn/Fe ratio (Figure 2). The surface area for the sample with a Zn/Fe ratio of 0.4 is almost twice that for Zn-free Fe_2O_3 (96 vs 53 m^2g^{-1}). The addition of K and/or Cu to Fe-Zn oxides did not influence surface areas, suggesting that K and Cu reside at Fe oxide crystallite surfaces and that they do not influence the structure or the dispersion of the Fe oxide phase. These data suggest that Zn as a $ZnFe_2O_4$ phase inhibits the sintering of Fe oxides, by keeping Fe oxides from migrating, and hence preventing sintering during treatments at high temperatures or by providing anchoring or nucleation sites for Fe oxides during precipitation or thermal treatment. However, it is not clear if this increase in surface area alone accounts for the higher FTS rates observed on Zn-promoted samples [14] or what the optimum Zn/Fe ratio is; therefore, the catalytic behavior of on K- and Cu-promoted Fe oxides with different Zn/Fe ratios was examined in order to establish a suitable Zn concentration for maximum FTS reaction rates.

Zn Promotion Effects on Fischer-Tropsch Synthesis Rates and Selectivity

Steady-state FTS rates and selectivities (493 K, 3.16 MPa) on Fe_2O_3-Zn-K-Cu catalysts with a constant K and Cu content (K/Fe=0.02, Cu/Fe=0.01) but different Zn contents are shown in

Table 1 at similar CO conversion levels. The presence of Zn at a Zn/Fe atomic ratio of 0.1 increased CO conversion rates (from 1.5 to 2.4 mol CO/h.g-at. Fe), but additional increases in the Zn/Fe ratio from 0.1 to 0.4 did not lead to higher FTS rates. The additional increase in surface area brought about by these higher Zn contents occurs at the expense of the reaction of some of the Fe oxide precursor to form less reducible $ZnFe_2O_4$. FTS selectivities (CH_4, C_{5+}, and *1*-pentene/*n*-pentane ratios) were almost unchanged by the presence of Zn. It appears that Zn acts only as a textural promoter and that a Zn/Fe atomic ratio of ~0.1 provides an optimum balance between a higher surface area and a decrease in the fraction of the Fe that is activated during contact with synthesis gas at F TS conditions. Therefore, a Zn/Fe atomic ratio of 0.1 was chosen to study the effects of Cu and K on FTS reaction rates and selectivities.

Reduction Kinetics of Fe_2O_3-Zn-K-Cu Precursors in H_2

Figure 3 shows the rates of removal of lattice oxygen atoms during treatment of Fe_2O_3-Zn-K-Cu precursors using H_2 as the reductant. The areas under these reduction peaks were calibrated using CuO. The respective amounts of oxygen in the two reduction peaks in Figure 3 show that Fe_2O_3 reduces in two steps. Fe_3O_4 is first formed and then reduced to form Fe metal. The presence of Cu in Fe-Zn oxides (Zn/Fe=0.1) causes the Fe_2O_3 reduction to Fe_3O_4 to occur at temperatures ~140 K lower than in Cu-free samples (Figure 3b); these reduction processes occur at temperatures identical to those required for the reduction of CuO to Cu metal (Figure 3a). As CuO reduces, Cu crystallites nucleate and provide H_2 dissociation sites, which in turn lead to reactive hydrogen species capable of reducing Fe oxides at relatively low temperatures. Potassium, shown to be present as a carbonate by X-ray absorption spectroscopy [22], does not influence the reduction of Fe_2O_3, but it weakly inhibits the reduction of Fe_3O_4 to metal Fe. When both Cu and K are present, the reduction profile resembles that for Fe_2O_3-Zn-Cu; Fe_2O_3 reduces at temperatures characteristic of CuO reduction (~470 K), except for a small fraction of the Fe_2O_3, which is not affected by Cu, apparently because of inefficient contact between some of the Fe_2O_3 precursor and the CuO promoter. The presence of Cu or K does not strongly influence the reduction of Fe_3O_4 to Fe, because thermodynamics and the nucleation of a new crystal structure, and not the H_2 dissociation steps, control reduction rates at these higher temperatures [23,24]. The effects of Cu on the kinetics of removal of lattice oxygen from Fe-Zn oxides suggest that Cu increases the initial rate of nucleation of reduced Fe oxide phases. Consequently, a larger number of nuclei become available for crystallization of reduced FeO_x and FeC_x crystallites; as a result higher FTS rates would be expected when precursor activation occurs in synthesis gas in the presence of these promoters.

Reduction and Carburization Kinetics of Fe_2O_3-Zn-K-Cu in CO

The rates of oxygen removal and of carbon introduction using CO were measured as a function of temperature on Fe_2O_3-Zn-K-Cu oxides by monitoring the concentrations of CO and CO_2 in the effluent stream. Two general stoichiometric reactions are involved in the carburization of Fe oxides. The removal of lattice oxygen occurs via the stoichiometry given by:

$$Fe_xO + CO = Fe_x + CO_2$$

Initially Fe oxides reduce to form CO_2 and a Fe center with valence lower than in Fe_2O_3. In a sequential or alternate step, CO carburizes Fe oxides to form CO_2 and Fe carbides:

$$Fe_xO + 2CO = Fe_xC + CO_2$$

In this step, oxygen removal and carbon deposition occur concurrently. The excess amount of CO consumed relative to the CO_2 produced provides a measure of the extent of carbon deposited. The different CO and CO_2 stoichiometries associated with these two steps, allows to decouple oxygen removal and carbon deposition steps using the following equations:

$$R_O = \text{Oxygen Removal Rate} = 2\, R_{CO2} - R_{CO} \qquad (1)$$

$$R_C = \text{Carbon Introduction Rate} = R_{CO} - R_{CO2} \qquad (2)$$

where, R_{CO2} is the rate of formation of the CO_2 product and R_{CO} is the rate of consumption of the CO reactant. We note that this approach remains rigorous even if the actual reactions do not proceed as written, because equations (1) and (2) merely reflect an oxygen and a carbon balance, respectively. Together with the structures detected by X-ray diffraction at various stages during reaction with CO, this approach probes the temperatures required, the rates of reduction and carburization, and the structure and stoichiometry of the carbides formed.

CO consumption and CO_2 formation rates are shown in Figure 4 for Fe_2O_3-Zn-K-Cu samples as a function of temperature. The stoichiometries for oxygen removal and carbon introduction measured from the areas under these peaks indicate that the reduction/carburization of Fe oxides proceeds in two sequential steps. Fe_2O_3 first reduces to Fe_3O_4 at ~543 K; then, Fe_3O_4 concurrently reduces and carburizes to a mixture of $Fe_{2.5}C$ and Fe_3C in the 543-723 K temperature range. Above 723 K, CO disproportionation occurs via the Boudouard reaction, with the formation of excess amorphous carbon; this amorphous carbon is not present in the carbide structures prevalent at temperatures below 723 K. X-ray diffraction patterns at various stages in these processes (Figure 5) confirmed the sequential nature of the structural evolution from Fe_2O_3 to Fe_3O_4 and then to mixtures of $Fe_{2.5}C$ and Fe_3C.

Figure 6 shows oxygen removal and carbon introduction rates as a function of temperature for Fe_2O_3-Zn-K-Cu samples using CO as the reactant. The areas under the oxygen removal peaks for Fe_2O_3-Zn confirm that Fe_2O_3 is first converted to Fe_3O_4 without any detectable carburization. The temperatures required and the areas under the carbon introduction peaks show that reduced Fe_3O_4 species are then concurrently carburized to form FeC_x (Figure 6a). The addition of K and/or Cu to Fe_2O_3 did not influence this reduction-carburization sequence, but the reaction rates increased and the required temperatures decreased when these promoters were present (Figure 6b-d). Cu increased oxygen removal rates and decreased the temperature required for the reduction and concurrent carburization of Fe_3O_4 by ~50 K. This effect of Cu on reduction rates was weaker than that observed when H_2 was used as the reductant, apparently as a result of the slower activation of CO relative to H_2 on Cu metal surfaces. The addition of K to Fe_2O_3 shifted the oxygen removal peak to higher temperatures (Figure 6c), but the rate of incipient carburization, indicated by the low-temperature shoulder in the carbon introduction peak, was slightly lower than on the unpromoted Fe oxide (Figure 6a). This may merely reflect a catalytic effect of K-promoted Fe oxides on CO activation rates [25] or just the faster nucleation of FeC_x

crystallites on oxide surfaces promoted with K carbonate. When both K and Cu were present in the catalyst, the combined effect of Cu in promoting the oxygen removal and K in CO activation least to the highest reduction/carburization and Fe carbide nucleation rates, as indicated by the markedly lowered temperatures required for oxygen removal and carbon introduction (Figure 6d).

In summary, K and Cu increase the rates of reduction and carburization of Fe-Zn oxide precursors when CO is used as the reactant, and the rate at which reduced Fe-containing phases (Fe_3O_4 or FeC_x) nucleate. These faster nucleation rates, in turn, appear to reflect a larger number of nucleation sites, which ultimately lead to smaller crystallites and to higher catalytic surface areas [17,19]. These promotional effects of K and Cu, which appear to be mostly textural in nature, are confirmed by the FTS catalytic data described in the next section.

Effects of K and Cu on Fischer-Tropsch Synthesis Rate and Selectivity

The promotion effects of Cu and K on the behavior of Fe-Zn catalyst for the FTS reaction were examined using a fixed-bed reactor with plug-flow hydrodynamics. Fe_2O_3-Zn catalysts (Zn/Fe=0.1) with different K (K/Fe=0, 0.02 and 0.04) and Cu (Cu/Fe=0, 0.01, 0.02) contents were evaluated at 493 K and 3.16 MPa. FTS rates and selectivities on these catalysts are shown in Table 2. CO conversion rates increased with the addition of K (K/Fe=0.02) or Cu (Cu/Fe=0.01), suggesting that the promotion of carburization and reduction rates by these species leads to either a larger number of active sites or to sites with a higher intrinsic activity. These rates were higher on the sample containing both K and Cu as promoters (Fe_2O_3-Zn-K_2-Cu_1) than on Cu-promoted (Fe_2O_3-Zn-Cu_1), K-promoted (Fe_2O_3-Zn-K_2), or unpromoted (Fe_2O_3-Zn) catalysts. The effects of K and Cu on the doubly promoted sample are nearly additive, suggesting an almost independent effect of the two promoters in increasing reaction rates. Previous studies on K-promotion on Fe-Si oxide catalysts showed a decrease in FT rates with increasing K concentration [16]. For the Fe-Zn oxide materials in this study, no detectable changes in FTS rates or selectivities were observed upon increasing the atomic K/Fe ratio above 0.02 (Table 2). Similarly, an increase in Cu/Fe atomic ratios from 0.01 to 0.02 did not influence reaction rates or product selectivities (Table 2). Thus, a Cu/Fe ratio of 0.01 and a K/Fe ratio of 0.02 appear to lead to optimum FTS catalytic properties, with further increases in the concentrations of promoters leading to negligible effects on both reaction rates and selectivities. It appears that the surface density of promoters or the extent to which they contact the Fe oxide precursors does not continue to increase as the Cu or K contents increase above a threshold value. This threshold value is most rigorously expressed as a promoter surface density and it corresponds to ~1 Cu/nm^2 and ~2 K/nm^2 [17].

Hydrocarbon formation rates (in mol CO/h.g-at. Fe) are shown in Figure 7 for the different K and Cu-promoted Fe_2O_3-Zn catalysts as a function of CO conversion. The effects of increasing CO conversion were similar on all catalysts, suggesting that these catalysts show similar kinetic dependences on reactant and product concentrations. CO_2 selectivities are shown as a function of CO conversion on these catalysts in Figure 8 and compared at a similar CO conversion value (14-18%) in Table 2. CO_2 selectivities increased with CO conversion on all four catalysts (Figure 8) and they were higher on Fe_2O_3-Zn promoted by both Cu and K than on unpromoted or singly promoted catalysts at all conversion levels. H_2O, which forms as a primary product during FTS on Fe catalysts, reacts with CO to give CO_2 via secondary water gas shift reactions. Davis *et al.* [27] identified a parallel pathway for CO_2 formation from alcohols (via aldehydes or acids) by the addition of isotopically labeled alcohols during FTS. For the catalysts and conditions of our studies, the oxygenate formation rates were much lower than the rates of secondary formation of CO_2, indicating that water gas shift reactions account for the observed increase in CO_2 selectivity with increasing residence time [28]. The local slope of the curves in Figure 8 reflect the contributions from secondary reactions (predominately water gas shift), while CO_2 selectivities extrapolated to zero conversion reflect the relative rates with which chemisorbed oxygen, formed in CO activation steps, is removed by CO instead of hydrogen. The slopes of the CO_2 selectivity curves in Figure 8 are similar for the K-promoted Fe_2O_3-Zn-Cu_1 and Fe_2O_3-Zn catalysts, indicating that these catalysts exhibit similar catalytic properties for secondary water gas shift reactions. Fe_2O_3-Zn and Fe_2O_3-Zn-Cu_1 catalysts without K also have nearly identical secondary water gas shift activity. These findings are somewhat unexpected in view of the high water gas shift rates reported on Cu-based catalysts [26]. The presence of Cu predominately influences the intrinsic oxygen removal selectivity by promoting the removal of oxygen using CO. On the other hand, Fe_2O_3-Zn-K_2 and Fe_2O_3-Zn-K_2-Cu_1 showed significantly larger slopes than K-free samples, indicating that the presence of K increases secondary water gas shift rates, as also reported previously on K-promoted Fe-Si catalysts [16], without influencing the primary oxygen removal selectivity.

The presence of K in Fe_2O_3-Zn catalysts led to lower CH_4 selectivities (Table 2, Figure 9) and higher C_{5+} selectivities (Table 2, Figure 10), apparently by decreasing the availability of H* atoms required for termination of growing chains via hydrogen addition reactions to form paraffins. In contrast, the addition of Cu to Fe_2O_3-Zn increased CH_4 selectivities and decreased C_{5+} selectivities (Table 2, Figure 10). When Cu and K are both present, the tendency of Cu to decrease product molecular weight almost disappears. In the presence of K, which promotes the chemisorption of CO and decreases H_2 dissociation, it is conceivable that the total H* surface coverage is very small because H_2 competes ineffectively with CO for adsorption sites.

Potassium also inhibits secondary reactions of α-olefins, such as isomerization to internal or branched olefins and hydrogenation to n-paraffins, by titrating certain acid or uncarbided sites on Fe_2O_3-Zn. The titration of these sites and the apparent decrease in the availability of adsorbed hydrogen also lead to lower rates of secondary hydrogenation reactions. *1*-Pentene/*n*-pentane ratios are shown in Figure 11 on several catalysts, and also compared in Table 2 at similar CO conversions. The olefin content on the K-promoted catalysts increased slightly with CO conversion. This is likely due to the inhibiting effect of H_2O or CO_2 on the termination of growing chains by hydrogen addition, as reported previously [14]. The intrinsic olefin/paraffin ratios (extrapolated to zero CO conversion) are actually higher for catalysts without K, but the tendency of such catalysts to hydrogenate olefins leads to a marked decrease in olefin content with increasing residence time. Taken together with the high CH_4 selectivities on Fe catalysts not promoted by K some surface regions with high local hydrogen to CO surface concentration and with a high concomitant activity for methanation and for olefin hydrogenation reactions. Similarly, *1*-decene/*n*-decane ratios (Figure 12, Table 2) are significantly higher in the presence of K and the effects of K are much stronger for the larger olefins, because of their greater propensity for secondary reactions. Hence, the inhibited hydrogen availability brought forth by K promotion has a greater impact on the heavier hydrocarbons formed in FTS.

Conclusions

Reduction-carburization studies showed that Fe_2O_3 sequentially reduces to Fe_3O_4 and then to a mixture of $Fe_{2.5}C$ and Fe_3C during activation in CO at 540-720 K. Precipitated Fe-Zn oxides form a mixture of Fe_2O_3 and $ZnFe_2O_4$. The latter inhibits sintering of Fe oxide phases at low Zn contents and provides a matrix for isolation of Fe_2O_3 at higher Zn contents, leading to an increase in surface area after thermal treatment and after activation in synthesis gas. Zn also reacts with Fe oxide precursors to form $ZnFe_2O_4$, a phase that does not reduce or carburize during FTS reactions. As a result, intermediate Zn/Fe ratios lead to optimum FTS rates, without any detectable changes in chain growth selectivity. Cu and K do not influence the surface area of Fe oxide precursors. Cu increases the rate of Fe_2O_3 reduction to Fe_3O_4 in H_2, while K promotes the activation of CO and the rate of carburization of Fe_3O_4. During activation in synthesis gas, the combined presence of K and Cu provides routes for the easier formation of Fe_3O_4 using H_2 and its faster carburization using CO. Cu and K both lead to the faster nucleation of oxygen-deficient Fe oxides and to the ultimate formation of smaller carbide crystallites with a higher active surface area. As a result, both Cu and K increase FTS rates on catalysts formed by activation in synthesis gas from Fe-Zn oxide precursors. Cu introduces sites with low chain growth probability and high olefin hydrogenation activity, but such sites appear to the poisoned by K. K and Cu also influence the mode of oxygen removal and the rate of secondary water gas shift. K increases water gas shift reaction rates, but it does not influence the relative rates at which chemisorbed oxygen is removed by CO or H_2 after CO activation steps. Cu increases the effectiveness of CO in this primary oxygen removal, but it does not influence the rate of the water gas shift reaction. K increases the olefin content and the average molecular weight of FTS products; and also titrates acid sites and inhibits H_2 dissociation.

Acknowledgements

The authors acknowledge financial support for this work by the U.S. Department of Energy, Division of Fossil Energy, under contract DE-FC26-98FT40308.

References

[1] Fischer, F., and Tropsch, H., *Brennstoff-Chem.* 7 (1926) 97.
[2] Anderson, R. B., in *Catalysis* Vol. 4, p. 29, Emmett, P. H., ed., Van Nostrand-Reinhold, New York, 1956.
[3] Storch, H. H., Golumbic, N., and Anderson, R. B., *The Fischer-Tropsch and Related Syntheses*, Wiley, New York, 1951; Anderson, R. B., *The Fischer-Tropsch Synthesis*, Wiley, New York, 1984.
[4] Dry, M. E., *The Fisher-Tropsch Synthesis*, in Catalysis-Science and Technology, Vol. 1, p. 160, Anderson, J. R., and Boudart, M., eds., Springer Verlag, New York, 1981.
[5] Kolbel, H., and Ralek, M., *Catal. Rev.-Sci. Eng.* 21 (1980) 225.
[6] Niemantsverdriet, J. W., and van der Kraan, A. M., *J. Catal.* 72 (1981) 385.
[7] Amelse, J. A., Butt, J. B., and Schwartz, L. J., *J. Phys. Chem.* 82 (1978) 558.
[8] Raupp, G. B., and Delgass, W. N., *J. Catal.* 58 (1979) 348.
[9] Dictor, R., and Bell, A. T., *J. Catal.* 97 (1986) 121.
[10] Reymond, J. P., Meriaudeau, P., and Teichner, S. J., *J. Catal.* 75 (1982) 39.
[11] Kuivila, S., Stair, P. C., and Butt, J. B., *J. Catal.* 118 (1989) 299.
[12] Huang, S., Xu, L., and Davis, B. H., *Fuel Sci. Tech. Int.* 11 (1993) 639.
[13] Iglesia, E., Reyes, S. C., Madon, R. J., and Soled, S. L., *Adv. in Catal.* 39 (1993) 221.
[14] Soled, S., Iglesia, E., Miseo, S., DeRites, B. A. and Fiato, R. A., *Topics in Catal.* 2 (1995) 193.
[15] Soled, S., Iglesia, E., and Fiato, R. A., *Catal. Lett.* 7 (1990) 271.
[16] Raje, A. P., O'Brien, R. J., and Davis, B. H., *J. Catal.* 180 (1998) 36.
[17] Li, S., Krishnamoorthy, S., Li, A., Meitzner, G. D., and Iglesia, E., *submitted to J. Catal.*
[18] O'Brien, R. J., Xu, L., Spicer, R. L., Bao, S., Milburn, D. R., and Davis, B. H., *Catal. Today* 36 (1997) 325.
[19] Li, S., Meitzner, G. D., and Iglesia, E., *J. Phys. Chem .B in press*.
[20] Li, S., Meitzner, G. D., and Iglesia, E., *submitted to J. Phys. Chem. B*.
[21] Lide, D. R.; Frederikse, H. P. R., Ed.; *Handbook of Chemistry and Physics*, 75th Ed.; The Chemical Rubber Company press: Boca Raton, 1994.
[22] Li, S., Meitzner, G. D., and Iglesia, E., *unpublished results*.
[23] Tiernan, M. J., Barnes, P. A., and Parkes, G. M. B., *J. Phys.Chem. B* 105 (2001) 220.
[24] Kung, H. H., *Transitional Metal Oxides*, *Stud. Surf. Sci. Catal.* 49 (1989).
[25] Somorjai, G. A., *Catal. Rev. Sci. Eng.* 23 (1981) 189.
[26] Habermehl, R., and Atwood, K., *Am. Chem. Soc. Div. Fuel. Chem. Prepr.* 8 (1964) 10.
[27] Davis, B.H., Xu, L., and Bao, S., Natural Gas Conversion IV, *Stud. Surf. Sci. Cat.* 107 (1997) 175.
[28] Krishnamoorthy, S., Li, A., and Iglesia, E., *manuscript in preparation*.

Table 1. Effect of Zn loading on the surface area and the steady state performance of a Fe_2O_3-K-Cu catalyst (K/Fe=0.02, Cu/Fe=0.01; H_2/CO=2, 493 K, 3.16 MPa, CO conversion=16-18%).

Sample	**Zn/Fe=0**	**Zn/Fe=0.1**	Zn/Fe=0.4
Surface area (m^2/g)	53	65	96
CO conversion rate (mol CO/h.g-at.Fe)	1.52	2.40	2.63
CO_2 formation rate (mol CO/h.g-at.Fe)	0.19	0.30	0.21
Hydrocarbon formation rate (mol CO/h.g-at.Fe)	1.33	2.10	2.52
CO_2 selectivity (%)	12.3	12.3	7.6
CH_4 selectivity (%)[a]	1.7	1.8	2.3
C_{5+} selectivity (%)[a]	86.6	87.6	85.6
1-C_5H_{10}/*n*-C_5H_{12} ratio	1.9	1.8	2.0

[a] CH_4 and C_{5+} selectivities are reported on a CO_2-free basis.

Table 2. Steady state performance of Fe_2O_3-Zn catalysts (Zn/Fe=0.1) with different loadings of K and Cu (H_2/CO=2, 493 K, 3.16 MPa, CO conversion = 14-18%).

K/Fe atomic ratio (×100)	0	0	2	2	2	4
Cu/Fe atomic ratio (×100)	0	1	0	1	2	1
CO conversion rate (mol CO/h.g-at.Fe)	0.70	0.87	1.23	2.40	2.43	2.49
CO_2 formation rate (mol CO/h.g-at.Fe)	0.02	0.06	0.10	0.30	0.32	0.30
Hydrocarbon formation rate (mol CO/h.g-at.Fe)	0.68	0.81	1.13	2.10	2.11	2.19
CO_2 selectivity (%)	2.3	6.5	8.5	12.3	12.9	12.1
CH_4 selectivity (%)[a]	4.8	10.2	1.8	1.8	2.0	2.5
C_{5+} selectivity (%)[a]	81.9	62.1	87.5	87.6	86.7	85.2
1-C_5H_{10}/*n*-C_5H_{12} ratio	1.9	1.7	1.8	1.8	1.8	2.0
1-$C_{10}H_{20}$/*n*-$C_{10}H_{22}$ ratio	0.4	0.4	1.7	1.8	1.7	1.7

[a] CH_4 and C_{5+} selectivities are reported on a CO_2-free basis.

Figure 1. X-ray diffraction patterns of Fe_2O_3-Zn samples with different Zn/Fe ratios. (a) 0, (b) 0.05, (c) 0.1, (d) 0.2, and (e) 0.4.

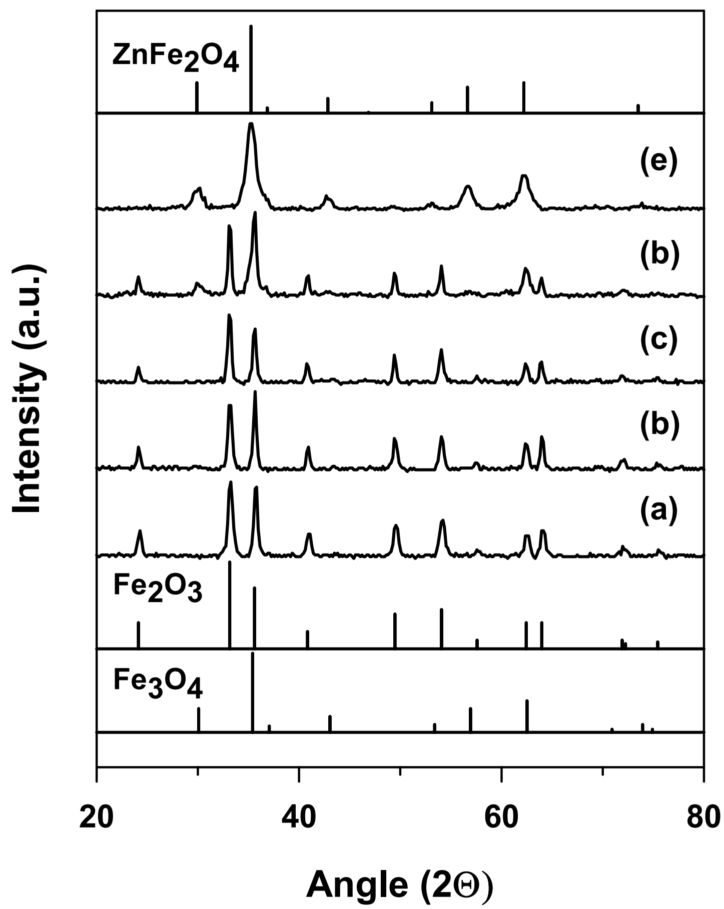

Figure 2. BET Surface areas of K- and/or Cu-promoted Fe_2O_3-Zn (K/Fe=0.02; Cu/Fe=0.01) samples as a function of Zn/Fe ratios: (●) Fe_2O_3-Zn-K_2-Cu_1 sample, (O) Fe_2O_3-Zn-Cu_1 sample, (□) Fe_2O_3-Zn-K_2 sample.

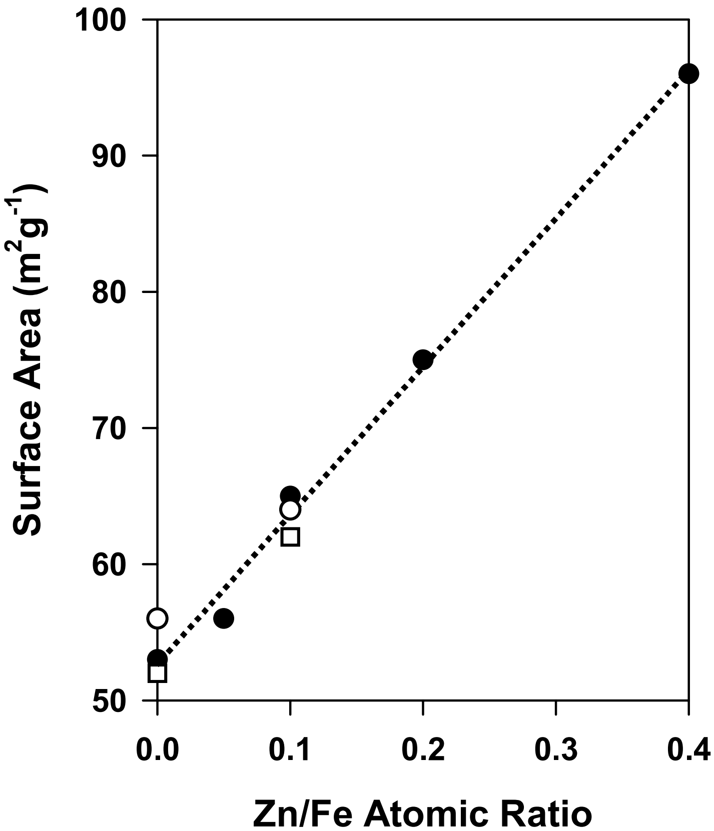

Figure 3. Oxygen removal rates of Fe_2O_3-Zn-K-Cu (Zn/Fe=0.1) in H_2. (a) CuO, (b) Fe_2O_3-Zn (c) Fe_2O_3-Zn-Cu_1, (d) Fe_2O_3-Zn-K_2, (e) Fe_2O_3-Zn-K_2-Cu_1 (0.2 g sample, 0.167 K/s ramping rate, 20% H_2/Ar, 0.268 mol/h flow rate).

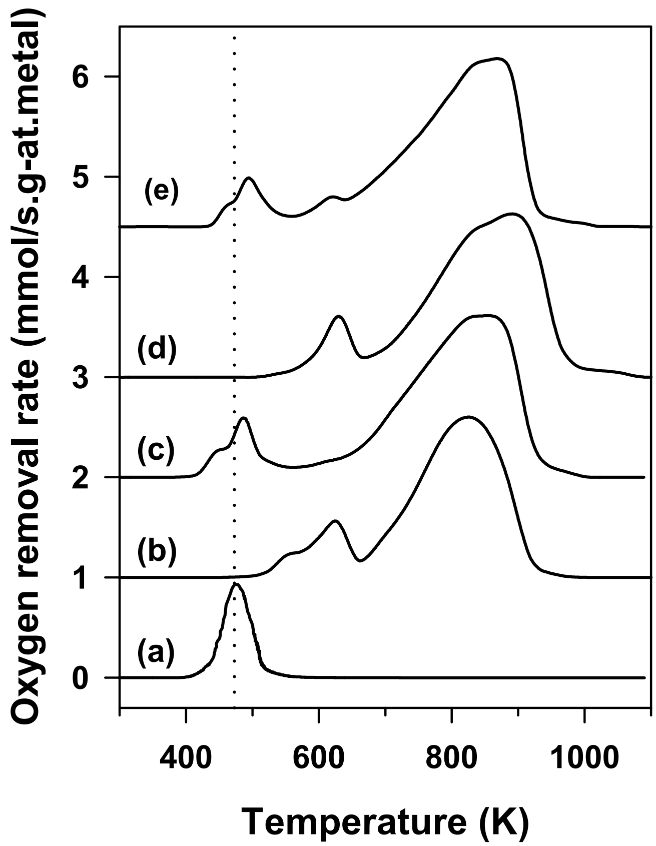

Figure 4. Rates of CO consumption (solid line) and CO_2 formation (dashed line) for the Fe_2O_3-Zn-K_2-Cu_1 sample (Zn/Fe=0.1) during the reduction and carburization in CO (0.2 g sample, 0.167 K/s ramping rate, 20% CO/Ar, 0.268 mol/h flow rate). Temperatures (dotted line) at which reactions were terminated for XRD measurements (Figure 5).

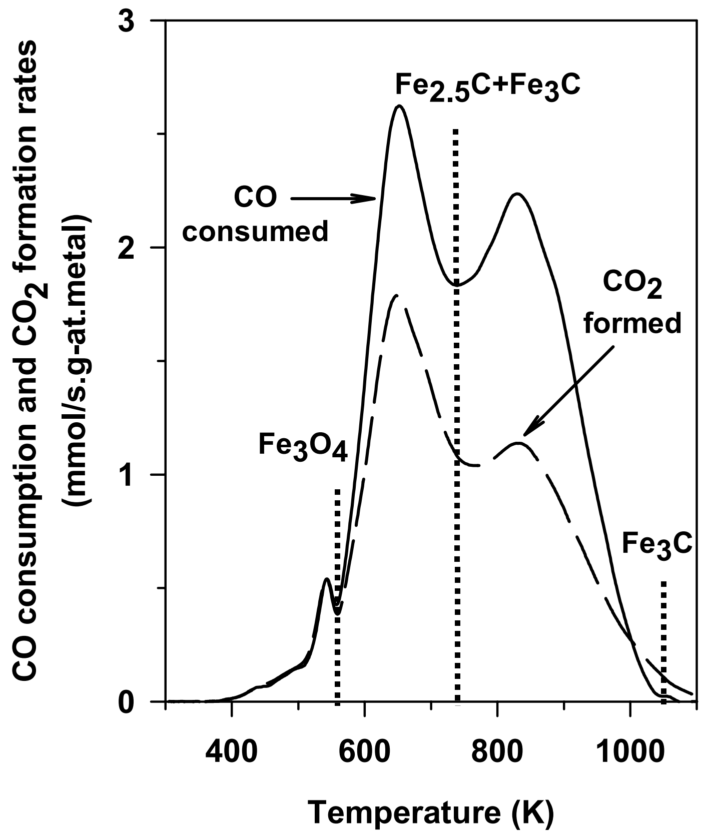

Figure 5. X-ray diffraction patterns showing the phase evolution of the Fe_2O_3-Zn-K_2-Cu_1 oxide (Zn/Fe=0.1) during the reduction and carburization in CO at (a) 560 K, (b) 730 K, and (c) >730 K (0.2 g sample, 0.167 K/s ramping rate, 20% CO/Ar, 0.268 mol/h flow rate).

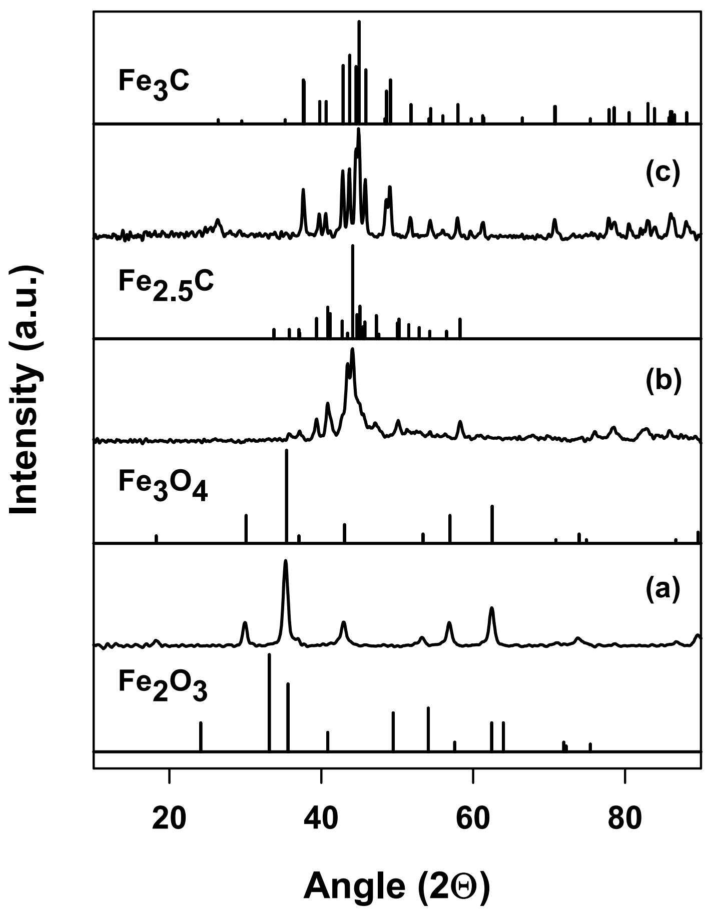

Figure 6. Oxygen removal and carbon introduction rates for the Fe_2O_3-Zn-K-Cu (Zn/Fe=0.1) samples in CO. (a) Fe_2O_3-Zn (b) Fe_2O_3-Zn-Cu_1, (c) Fe_2O_3-Zn-K_2, (d) Fe_2O_3-Zn-K_2-Cu_1 (0.2 g sample, 0.167 K/s ramping rate, 20% CO/Ar, 0.268 mol/h flow rate)

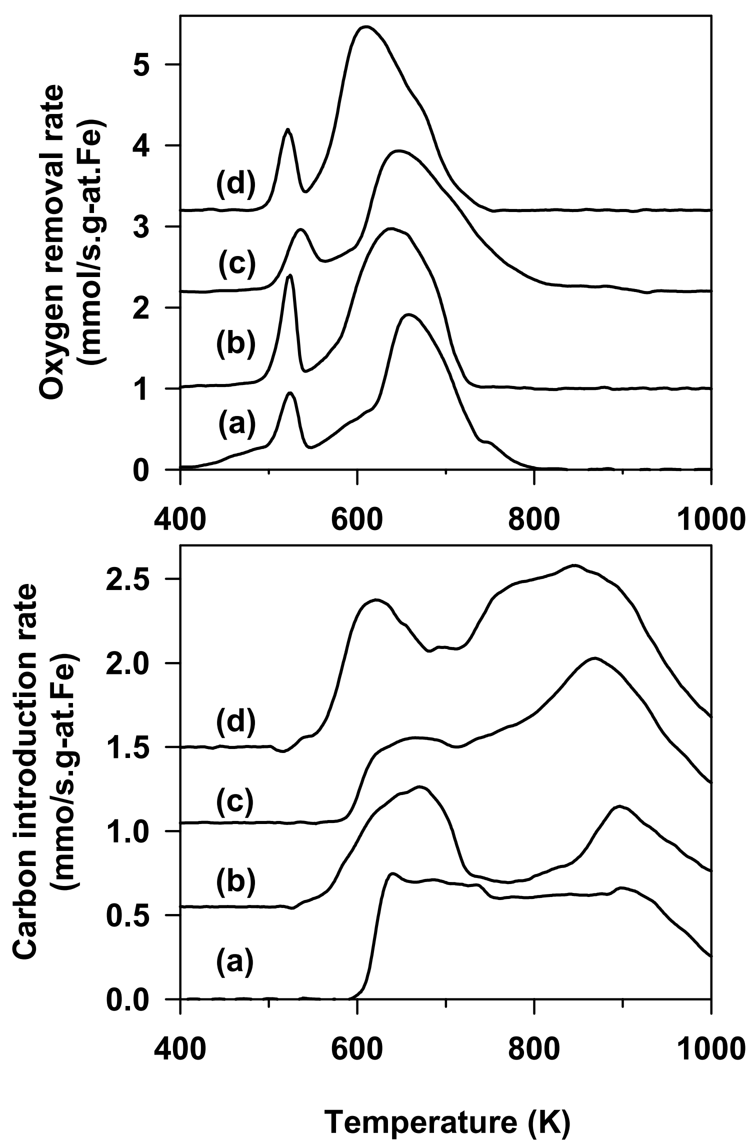

Figure 7. Hydrocarbon formation rates on Fe_2O_3-Zn (●), Fe_2O_3-Zn-Cu_1 (▲), Fe_2O_3-Zn-K_2 (◆), and Fe_2O_3-Zn-K_2-Cu_1 (■) catalysts (493 K, 3.16 MPa, H_2/CO=2).

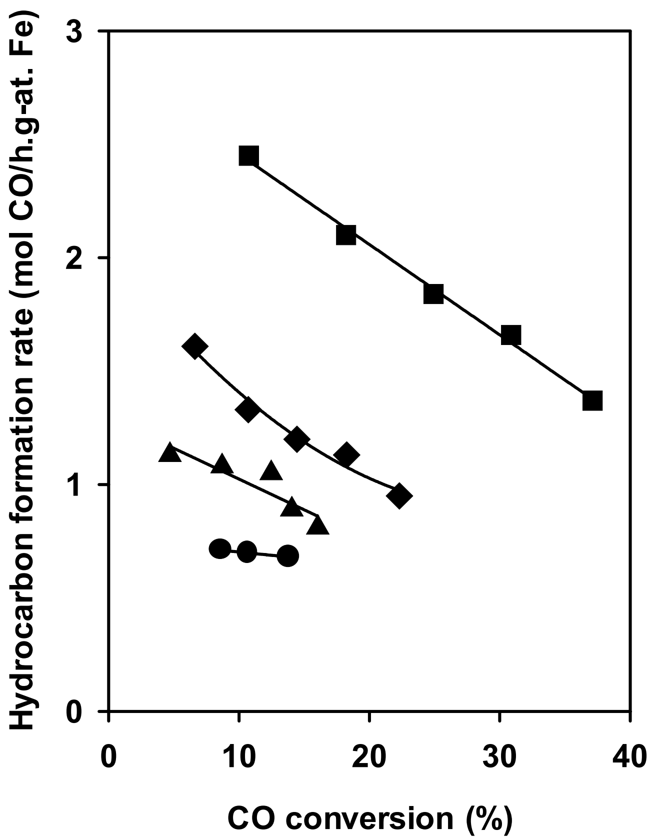

Figure 8. CO_2 selectivities on Fe_2O_3-Zn (●), Fe_2O_3-Zn-Cu_1 (▲), Fe_2O_3-Zn-K_2 (◆), and Fe_2O_3-Zn-K_2-Cu_1 (■) catalysts (493 K, 3.16 MPa, H_2/CO=2).

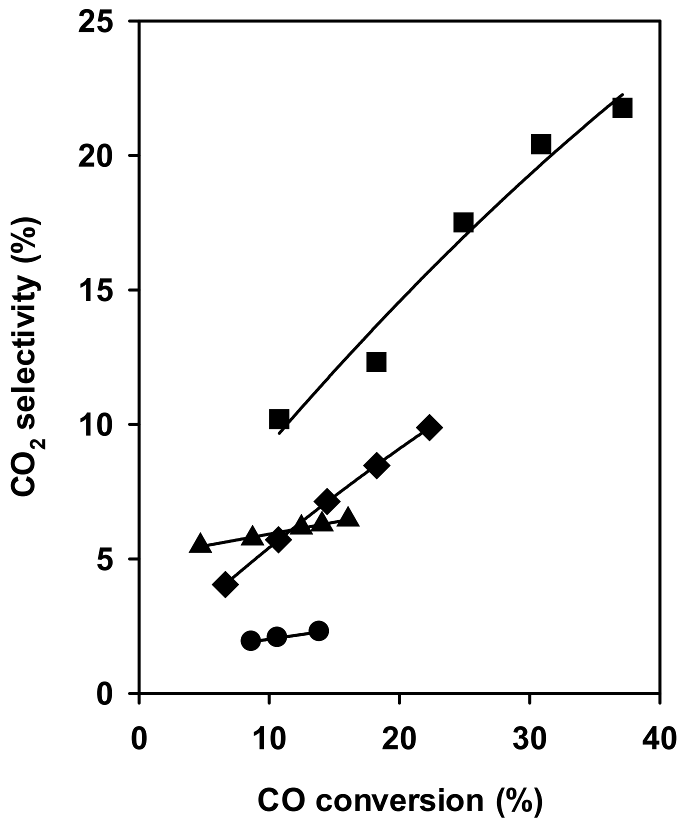

Figure 9. CH_4 selectivities on Fe_2O_3-Zn (●), Fe_2O_3-Zn-Cu_1 (▲), Fe_2O_3-Zn-K_2 (◆), and Fe_2O_3-Zn-K_2-Cu_1 (■) catalysts (493 K, 3.16 MPa, H_2/CO=2).

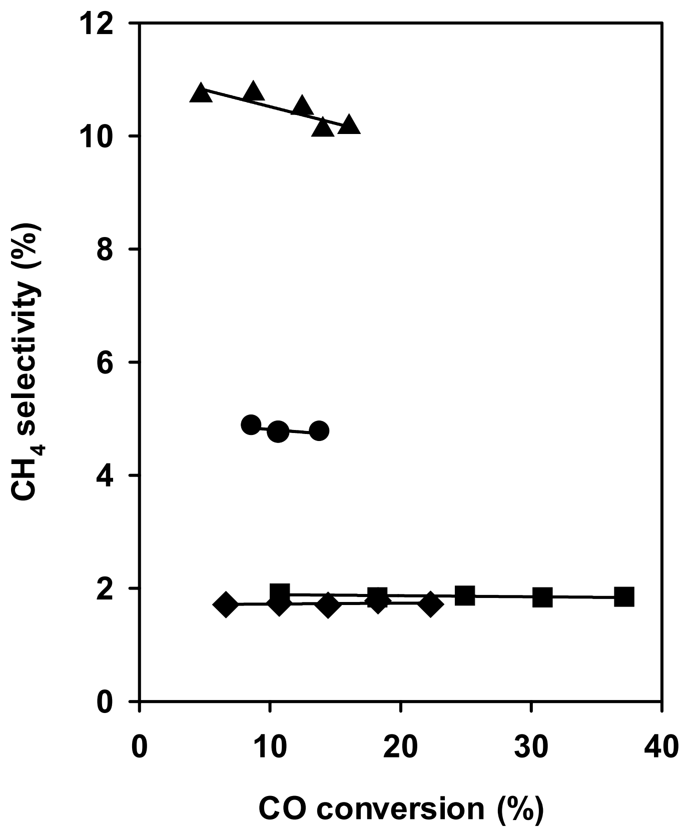

Figure 10. C_{5+} selectivities on Fe_2O_3-Zn (●), Fe_2O_3-Zn-Cu_1 (▲), Fe_2O_3-Zn-K_2 (◆), and Fe_2O_3-Zn-K_2-Cu_1 (■) catalysts (493 K, 3.16 MPa, H_2/CO=2).

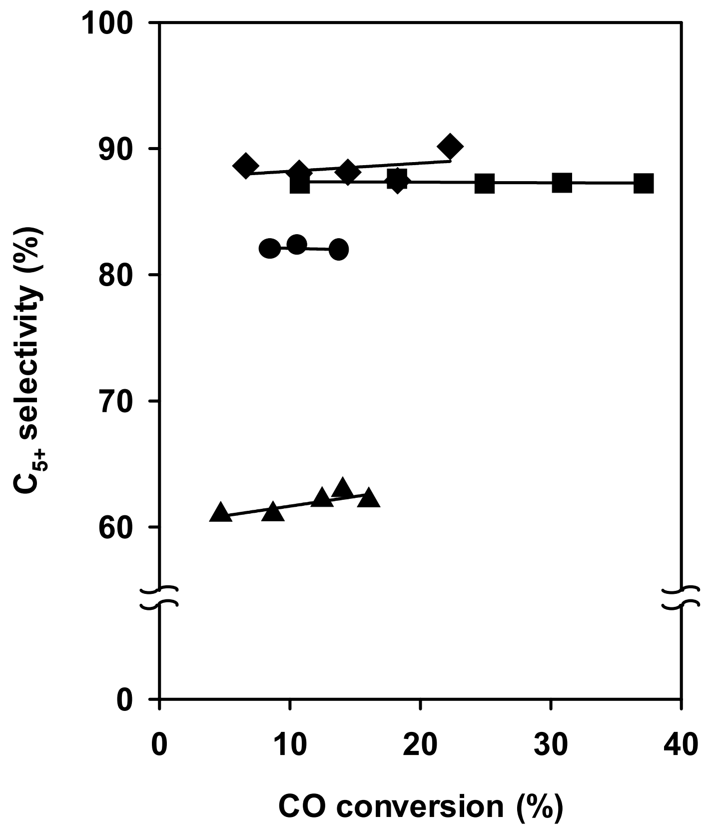

Figure 11. *1*-C_5H_{10}/*n*-C_5H_{12} ratios on Fe_2O_3-Zn (●), Fe_2O_3-Zn-Cu_1 (▲), Fe_2O_3-Zn-K_2 (◆), and Fe_2O_3-Zn-K_2-Cu_1 (■) catalysts (493 K, 3.16 MPa, H_2/CO=2).

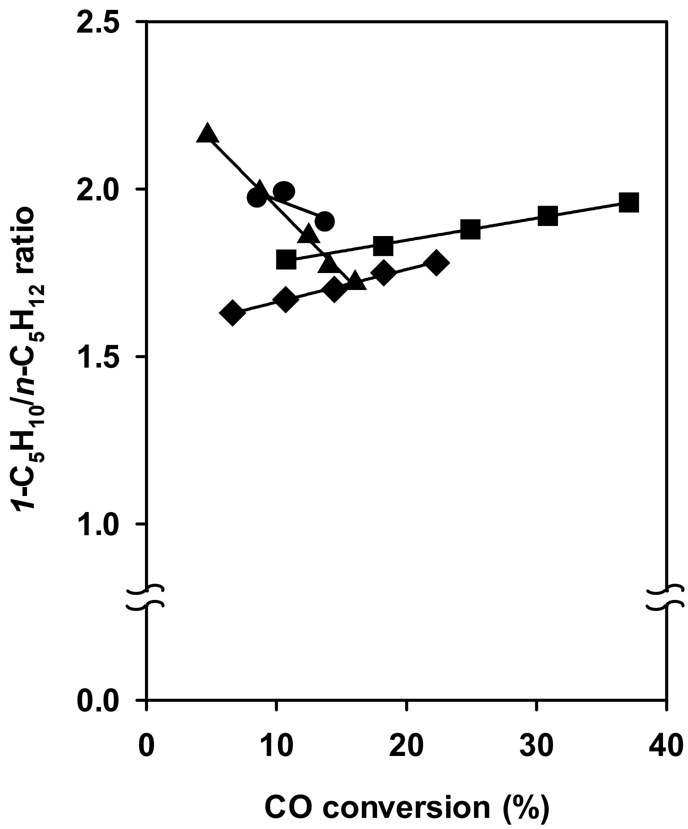

Figure 12. 1-$C_{10}H_{20}$/n-$C_{10}H_{22}$ ratios on Fe_2O_3-Zn (●), Fe_2O_3-Zn-Cu_1 (▲), Fe_2O_3-Zn-K_2 (◆), and Fe_2O_3-Zn-K_2-Cu_1 (■) catalysts (493 K, 3.16 MPa, H_2/CO=2).

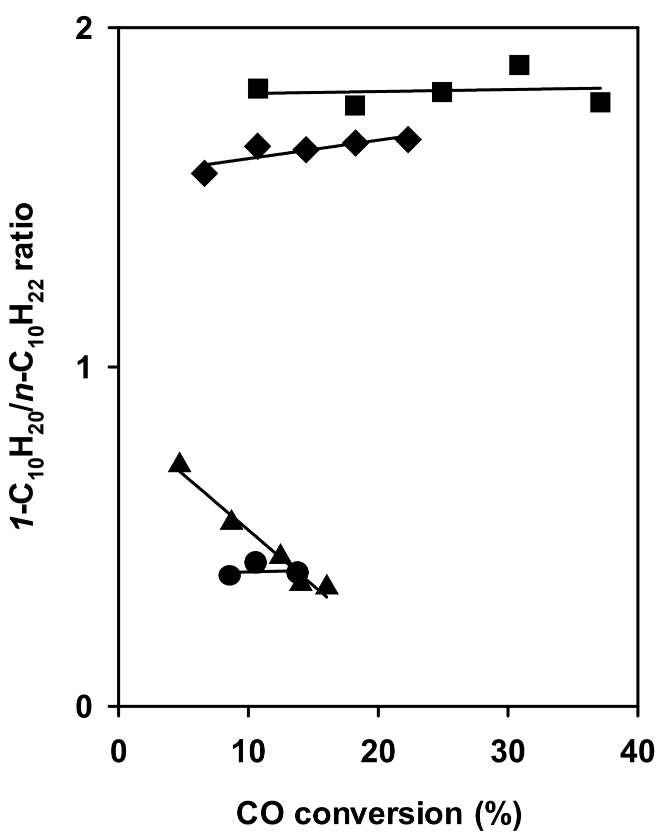

4.2. Steady-state Transient Isotopic Labeling Experimental Setup

The layout of the setup is illustrated in Fig 1. The first unit of the system on right side is the gas-feeding manifold. The system is equipped with independent, MFC controlled gas feed lines. The feed lines are grouped into two branches, Line 1 and Line 2. Line 1 delivers the non-labeled and pure gases, Line 2 the labeled ones and mixtures. The hydrogen feed in Line 2 contains 5% helium as hydrodynamic tracer. The calibration bridge is used for calibrate the step switch between the two lines. The bridge makes possible to feed in the two lines simultaneously at known percentage ratio. Varying the ratio of the two lines between 0 and 100% provides the step response calibration for both the ^{13}CO and He step.

The next major unit is the reactor–bypass structure. The loops start and end in two four way valves (FWV1 and FWV2). In the bypass branch there is a needle valve to balance the pressure between the two loops. It is important that step like forcing input can be imposed on the flow by both of the four way valves. With the help of the valve FWV2, the disturbing effects upstream and downstream can be eliminated.

The third unit is the analysis system. Two-stage pressure reduction is applied to reduce the pressure from working condition down to 10^{-3} Pa where the mass spectrometer can operate. Two kinds of capillaries can be applied between the two split chambers. It can be either an empty stainless steel or a fused silica with dispersed Pt inside coating. By the help of the latter, all the hydrocarbon products can be oxidized into CO_2 and in this way total carbon balance can be obtained. In this case O_2 make up gas has to be supplied.

The transient measurement requires exact mass balance calculations. This can be done easily if the reactor is operating as a CSTR unit. In order to fulfill this condition a new fluidized bed micro reactor was designed and manufactured. The design is plotted in Fig. 2. The reactor has two 1/16" OD capillary-like inlets and one 1/8" outlet. The two inlets form an expanding jet flowing from opposite directions. The direction of the outlet is reversed compared to one of the inlet.

Figure 1. Steady-state transient labeling experimental setup.

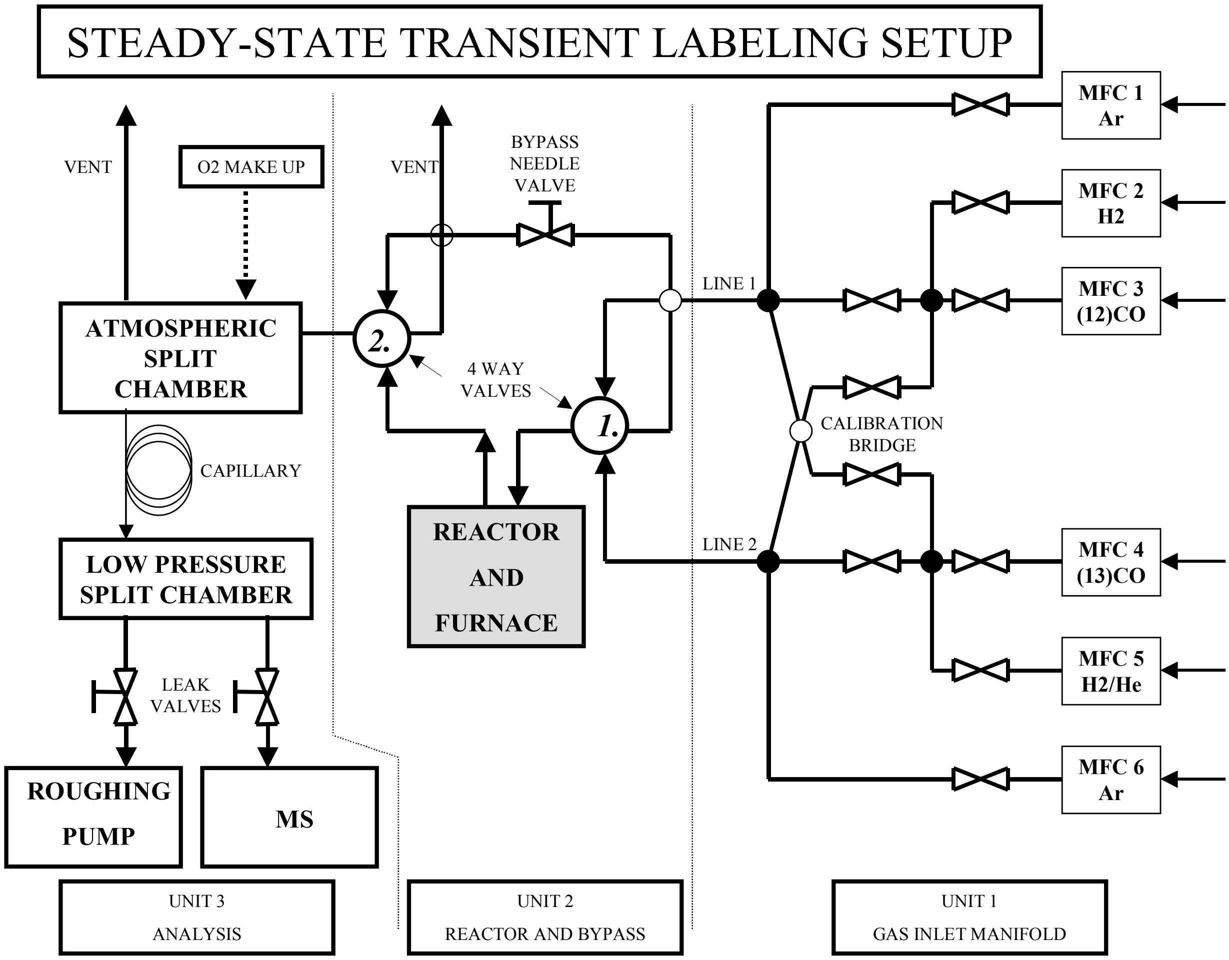

Figure 2. Fluidized bed micro reactor.

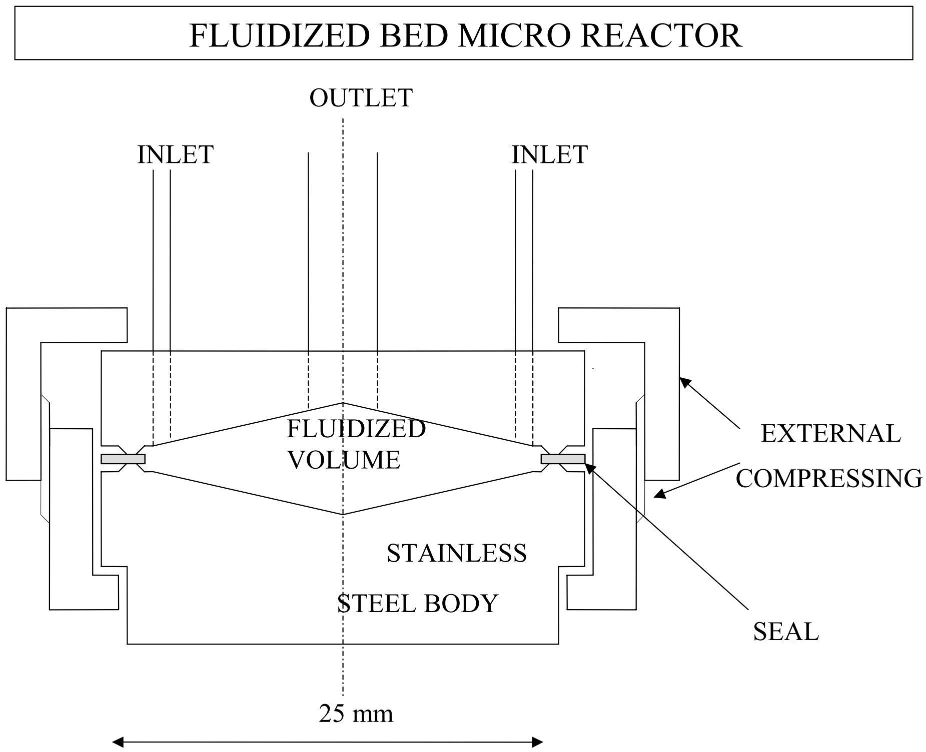

5. FISCHER-TROPSCH SYNTHESIS ON FE-BASED CATALYSTS

5.1 CO_2 formation and its abatement by recycle on Fe-based FTS catalysts

Abstract

The role of promoters such as Cu and K used in Fe-based Fischer Tropsch Synthesis (FTS) catalysis, on CO_2 formation has been investigated. These promoters affect the relative probability of O* removal by either CO, a primary pathway or by water, a secondary pathway. K appears to promote the secondary water-gas shift reaction while Cu addition appears to promote the primary pathway The effect of CO_2 addition on the hydrocarbon product selectivity for the Fischer-Tropsch Synthesis, as well as its role in the control of the concurrent water gas-shift reaction, has been investigated over a number of Fe-Zn catalysts promoted with Cu, Ru and K at 543 K and 0.5 MPa. The addition of CO_2 to synthesis gas decreased CO_2 formation on all catalysts by increasing the rate of the reverse step of the Water Gas-Shift (WGS) reaction and pushing the reaction towards equilibrium. However, no effect on the forward rate of the WGS reaction or FTS rate was observed indicating that CO_2 dissociation is largely an irreversible step. CO_2 addition also led to an increase in the olefin selectivity in the FTS product distribution, due to a decrease in the effective hydrogen surface concentration on the catalyst and had a small increase in the selectivity to high molecular weight hydrocarbons. Our studies demonstrate that CO_2 recycle can be used a tool in commercial FTS reactors in order to improve the overall carbon efficiency of synthesis gas towards the desired hydrocarbon products.

Introduction

The Fischer-Tropsch Synthesis reaction converts synthesis gas, *i.e.*, a mixture of CO and H_2 (derived from coal or natural gas), into a range of hydrocarbons comprising of liquid fuels such as gasoline and chemicals such as *1*-alkenes, which are valuable raw materials for several down-stream processes [1-5]. The catalysts that are typically employed in FT synthesis are Group VIII metals such as Fe, Co and Ru [2-5]. The use of Fe catalysts for FT synthesis stems from their easy availability and low cost, which makes them economically attractive, and their flexibility in terms of operating conditions and product distribution. Fe catalysts usually employ one or more of promoters such as SiO_2, ZnO, CuO, K_2O etc., which play key roles in promoting the catalyst activity and product selectivity for the FTS reaction [6-8]. Oxides such as MnO_x and ZnO help to preserve the Fe-structure, while CuO helps in the reduction process of the catalyst and hence promotes the FTS reaction rate. Alkali promoters promote CO dissociation and cause an increase in the concentration of the active surface carbon species, which in turn results in an increase in the olefin selectivity and the formation of high molecular weight products.

The oxygen resulting from CO dissociation on the catalyst surface during FTS reaction can be scavenged in one of two ways. It can either react with surface hydrogen to form water, or react with CO to form CO_2, both of these being primary reactions. CO_2 can also be formed *via* a secondary reaction between CO and H_2O, *i.e.*, the WGS reaction [5,9,10]. Thus, the total CO_2 formation can be interpreted as the sum of the CO_2 produced from the primary and secondary reactions.

Fe-based catalysts exhibit a high selectivity to CO_2, owing to the fact that Fe, Zn and Cu oxides present in the catalyst system have good WGS activity [9-11]. Such an effect can be beneficial when operating the FTS reaction with a coal-derived syngas (with a H_2/CO ratio of 0.67). Since the FTS reaction rate has a positive order dependence on the hydrogen partial pressure, an enhancement in the hydrogen concentration due to the WGS reaction can lead to higher FT rates. On the other hand, a high CO_2 selectivity is detrimental when operating with a hydrogen-rich synthesis gas such as the one derived from natural gas (H_2/CO=2.0), since it can lead to lower hydrocarbon productivity (due to a higher utilization of CO to form CO_2). In addition, a high CO_2 selectivity also indicates a higher surface H_2/CO ratio, which could result in a very high methane yield and a reduction in the production of high molecular weight hydrocarbons. The production of CO_2 also increases with increasing temperature and this will have a bigger impact when FTS reaction is operated at conditions ideal for the synthesis of low and intermediate molecular weight olefins. Hence, the key to the design of a good Fischer-Tropsch catalyst is the minimization of CO_2 formation to achieve high hydrocarbon yields.

The mechanism of formation of CO_2 and its effect on chain growth has been a subject of debate in the literature. Some researchers have concluded that FTS and WGS reactions take place on different sites on Fe catalysts [11-13]. It was proposed that the Fe carbide phase has a low WGS activity and a high FTS activity, while the magnetite phase (Fe_3O_4) has a high WGS activity and negligible FTS activity. Another group proposed the WGS reaction rate is determined by the rate of formation of a surface formate ($HCOO^-$) intermediate [14]. The presence of different additives in the Fe catalysts can also influence the mode of CO_2 removal. However, temperature-programmed measurements and in situ X-ray absorption studies conducted by Li and co-workers have shown that FTS reactions on Fe-based catalysts essentially involve surface Fe carbides and its neighboring surface vacancies [15]. Since the catalyst surface has dissociated CO and H_2 leading to the formation of CH_x monomers, it is unlikely that CO_2 formation can be associated with a different Fe site. Recently, Davis *et al.* with addition of ^{14}C-labeled alcohols to syngas during FTS, at conditions close to WGS equilibrium, showed that the ^{14}C content in CO_2 was significantly higher than that of CO, which indicated that CO_2 could be produced from alcohols as well as from the water-gas shift reaction [16]. Xu *et al.* also showed via the addition of $^{14}CO_2$ to synthesis gas during FTS that CO_2 can initiate chain growth in a pathway independent from that occurring from CO, but does not participate in chain propagation [17]. They proposed that CO_2 hydrogenation could independently produce alcohols that lead to the formation of hydrocarbon chains.

The WGS reaction is an equilibrium-controlled reaction and hence the formation of CO_2 can be minimized by increasing the rate of the reverse reaction with the possible addition of CO_2, and hence push the reaction closer to equilibrium. One possible approach is to recycle CO_2 produced during the FTS reaction back to the feed stream. Soled *et al.* performed CO_2 addition studies on Fe-Zn catalysts and observed a significant decrease in CO_2 production [18]. However, no further details including the selectivity effects and mechanistic role of CO_2 were reported.

In this work, we discuss the role of different additives (CuO and K_2CO_3) on CO_2 formation during FTS reactions. We also demonstrate the existence of two possible routes of CO_2 formation based on our $^{13}CO_2$ addition studies at conditions where the WGS reaction is far away from equilibrium. In addition, the possibility of CO_2 addition/recycle as a tool for minimization of the overall CO_2 formation, FTS reaction kinetics, hydrocarbon product distribution and the olefin content was also studied at 508 K and 2.14 MPa and the results are presented in this work.

Experimental Approach

Catalyst Preparation

All the catalyst used in this work were prepared by the co-precipitation of Zinc and Iron nitrates at a constant pH (7.0) to form porous mixed oxides, followed by successive impregnation with aqueous solutions of copper nitrate and potassium carbonate (for promotion) to incipient wetness. The details of the preparation procedure and post-preparation treatment (drying and calcinations protocols have been described elsewhere [6,7].

Reaction system

Fischer-Tropsch synthesis was performed in a fixed-bed, single-pass SS-304 (1/2"×0.028") flow reactor, housed in a three-zone furnace (ATS 302C Series 3210), with 0.4 g of the catalyst sample (80-140 mesh and diluted with ~11 g quartz chips). The presence of the diluent served to prevent temperature gradients, and the axial temperature was found to be within ±0.5 K of the average value as monitored by a moving thermocouple. Synthesis gas (62/31/7 mol %H_2/CO/N_2, Praxair, N_2 as the internal standard), was purified by passing through a metal carbonyl trap (Sorb-Tech RL-13, activated carbon) and a water trap (Matheson 452 A, 4A molecular sieve). A certified mixture of 50% CO_2: 50% Ar (Linde Air Products Co.) was used for the CO_2 addition experiments with Ar being used as the internal standard for CO_2. For $^{12}CO_2$ and $^{13}CO_2$ addition studies, the partial pressures of $^{12}CO_2$ and $^{13}CO_2$ (Cambridge Isotope Laboratories Inc., 99%) were varied while holding the partial pressures of CO and H_2. The reactor pressure was maintained using a dome-loaded backpressure regulator (Mity Mite Model S-91xw). All lines from the reactor outlet were heat traced to 433-453 K. The catalysts were activated *in situ* in synthesis gas at 0.1 MPa by increasing the temperature from 293 K to 543 K at a rate of 0.017 K/s. After holding it at 543 K for about 0.5 h, the reactor temperature and pressure were set to the desired conditions.

The feed gas and reactor effluent were analyzed on-line using a gas chromatograph (Hewlett Packard, Model 5890 Series II). All hydrocarbon products were analyzed using a flame ionization detector and a HP-1 capillary column (cross-linked methyl silicone, 50 m × 0.32 mm × 1.05 μm) while the rest of the components along with CH4 were analyzed using a thermal conductivity detector and a Porapak Q (15.2 cm × 0.318 cm) packed column. For determining the ^{13}C content in the product stream, CO and CO_2, samples were injected into a Gas chromatograph coupled with a Mass Selective Detector (Hewlett Packard, Model 5890 Series II/5791A) and a HP-1 capillary column (cross-linked methyl silicone, 50 m × 0.32 mm × 1.05 μm).

Results and Discussion

Role of additives on CO_2 formation - Effect of CuO and K_2CO_3:

The CO_2 selectivity on the Fe-Zn-K (Zn/Fe=0.1, K/M=0.02; M=Zn+Fe and Fe-Zn-K-Cu (Zn/Fe=0.1, Cu/M=0.01, K/M=0.02; M=Zn+Fe) catalysts at 508 K and 2.14 MPa, are shown as a function of CO conversion in Figure 1a. The CO_2 selectivity increases with increase in CO conversion in all three cases. The overall CO_2 selectivity at a given CO conversion is highest on catalysts promoted with both Cu and K and lowest on Fe-Zn. Both Fe-Zn-K and Fe-Zn-K-Cu appear to have selectivity curves with nearly identical slopes. Similarly the Fe-Zn-Cu and Fe-Zn catalysts also have nearly identical slopes. The slope of the CO_2 selectivity curve is a measure of the secondary WGS reaction, is almost identical for all the three catalysts, indicating that the addition of Cu to Fe-Zn-K or Fe-Zn does not enhance the removal of O* by H*. Rather, the y-intercept of the selectivity curves, which is a measure of the primary CO_2 formation rate, is higher when Cu is present. Thus the presence of Cu appears to promote the removal of O* by CO*. The presence of K promotes the dissociation of CO to form surface carbidic species and hence it is conceivable that the catalyst surface is covered mostly by surface carbide and not CO which would be necessary for O* removal *via* the primary route. In the presence of Cu oxides, it appears that there is an increase in the CO* concentration available for O* removal. Previous studies with supported Cu catalysts have also shown that Cu-based catalysts assist CO_2 formation by CO* and O* as well as by the WGS reaction [19]. Metals such as Cu have a higher tendency to associatively adsorb CO than Fe, based on infrared studies, which show an increase in the vibrational frequency of the C-O bond Cu to Fe [20]. Hence there is a possibility of a higher availability of CO* for primary CO_2 formation. With increase in temperature to 543 K (Figure 1b), the slope of the CO_2 selectivity curve decreases for catalysts that approach WGS equilibrium. Fe-Zn-K-Cu indicating the approach of the secondary water gas-shift reaction closer to equilibrium in these cases (Figure 1b). Also, the removal of O* by CO*, represented by the y-intercept of the CO_2 selectivity curve, increases with increasing temperature on all catalysts. This is likely to an increase in the rate of CO disproportionation on the catalyst leading to the deposition of C* and simultaneous formation of CO_2.

Davis *et al.* with addition of ^{14}C-labeled alcohols during FTS showed that CO_2 could be produced from alcohols as well as from the water-gas shift reaction [16]. They proposed that alcohols could lead to aldehydes via oxidation and further to acids before they can undergo decarbonylation to give CO_2 and an alkane as shown below.

$$\mathrm{RCH_2OH} \Leftrightarrow \mathrm{RCHO} \Leftrightarrow \mathrm{RCOOH} \Leftrightarrow \mathrm{RH} + \mathrm{CO_2}$$

However, we observed smaller amounts of oxygenates (alcohols, ketones, aldehydes and acids) formed under our reaction conditions, likely due to a higher H_2/CO ratio used in our case (2 vs 0.7 used by Davis *et al.*) which results in a lower probability for CO insertion steps into growing chains. Figure 2 shows the total selectivity to oxygenates (C_2-C_{13}) and CO_2 as a function of CO conversion on the Fe-Zn-K-Cu catalyst at 508 K and 2.14 MPa. The selectivity to oxygenates decreases with CO conversion due to the existence of secondary reactions including conversion to alkanes and CO_2. Since one mole of an oxygenate compound (>C_1) can lead to one mole of CO_2 via the above mentioned reaction, the amounts of oxygenates extrapolated to zero CO conversion are insufficient to explain the total amount of CO_2 formed under the same conditions, which indicated that their contribution to CO_2 formation is very small compared to that of CO.

CO_2 addition effects on Fe-based catalysts for FT synthesis:

The water gas-shift reaction is limited by equilibrium [9,10] and one measure of the distance of this reaction away from equilibrium can be obtained by the following ratio,

$$\eta = \frac{\left(\frac{P_{CO_2} P_{H_2}}{P_{CO} P_{H_2}} \right)}{K} \tag{1}$$

where, the P-terms represent partial pressures of the individual gases and K is the equilibrium constant for the WGS reaction at the reaction temperature. To minimize the utilization of CO towards the formation of CO_2 and hence improve the overall carbon efficiency, the WGS reaction has to be operated close to its equilibrium. This could be achieved by the addition of CO_2 pressure as indicated by the approach of η towards 1 as illustrated in Figures 3a and 3b at different temperatures.

CO_2 addition experiments (0 to 0.4 MPa) were conducted on the Fe-Zn-K-Cu catalyst at 543 K and 0.5 MPa. The CO and the syngas ($CO+H_2$) conversions obtained on the Fe-Zn-K-Cu catalyst as a function of the CO_2 pressure added are shown in Figures 4a and 4b at 508 K and 543 K respectively. The CO conversion showed a gradual decrease with increasing CO_2 pressure, which indicates that the addition of CO_2 decreases the utilization of CO towards forming CO_2 via the water-gas shift reaction. The effects are larger at the higher temperature due to the approach towards equilibrium. However, the syngas conversion was independent of CO_2 pressure indicating that dissociation of CO_2 under these conditions (*i.e.* below WGS equilibrium) is a slow process and hence does not eventually contribute to a significant amount of -CH_2-monomers formed. This is also illustrated by the similar decreases in the CO conversion rate and CO_2 formation rate as a function of the amount of added CO_2 compared with nearly unchanged hydrocarbon formation rate, in Figures 5a and 5b.

CO_2 formation rate *via* the secondary WGS reaction depends on the CO_2 forward rate r_f, and reverse reaction rate r_b, and can be expressed as follows:

$$r = r_f - r_b = k_1 f(P_j) - k_{-1} g(P_i) \tag{2}$$

where, k_1 is the rate constant for the forward reaction and k_{-1} the rate constant for the reverse reaction. Since $r_f = r_b$ at equilibrium, the reaction rates must satisfy the equation,

$$\frac{f(P_j)}{g(P_i)} = \frac{P_{CO_2} P_{H_2}}{P_{co} P_{H_2O}}. \tag{3}$$

Then from equations (1), (2), and $K = k/k_{-1}$, we can obtain the following equation.

$$r = k_1 f(P_j)(1 - \frac{k_{-1}}{k_1}\frac{f(P_j)}{g(P_i)}) = r_f(1-\eta) \quad (4)$$

Figure 6a and 6b show the CO_2 forward rate r_f (= $r/(1-\eta)$) as a function of amount of CO_2 added at 508 K and 543 K. It is seen that CO_2 forward rate r_f was almost unchanged within the experimental error. Therefore, the reduction in CO_2 net formation rate is caused by the increase in the reverse rate of water-gas shift reaction after addition of CO_2 and does not change the rate of the forward step of the WGS reaction. The extrapolation of the CO_2 rate curve (Figure 6b) to the zero on the x-axis showed that a CO_2/CO ratio of 5.5 is required for the complete elimination of CO_2 formation at 543 K, while the theoretical value from equilibrium calculations was 5.2.

The effect of added CO_2 on the product selectivities was also studied. The selectivity of CO_2, CH_4 and C_{5+} (the last two calculated on a CO_2-free basis) are shown as a function of the CO_2 pressure in Figures 7a and 7b. An increase in the reverse rate of the water gas-shift reaction leads to a decrease in the H* availability on the surface, which in turn results in a decrease in the CH_4 selectivity and an increase in the C_{5+} selectivity in the case of Fe-Zn-K-Cu. However, this change is not pronounced since the majority of the surface active sites are covered with CO* under these conditions due to the ability of K to promote CO chemisorption and inhibit hydrogen chemisorption [6]. Concurrently, the α-olefin/*n*-paraffin ratios on the Fe-Zn-K-Cu catalyst should increase with increasing CO_2 pressure (Figures 8a and 8b). These ratios increased for all the carbon numbers at 543 K with increasing CO_2 pressure. However, the effects were very small at 508 K because of the distance away from WGS equilibrium. A negative slope for the α-olefin/*n*-paraffin ratio indicates the existence of secondary reactions namely hydrogenation and α-olefin readsorption, whereas the y-intercept is a measure of the relative probability of intrinsic termination to an α-olefin or a *n*-paraffin. These ratios increased upon CO_2 addition indicating an inhibition effect on paraffin formation in the hydrocarbon product distribution. Similar paraffin inhibition has previously been observed on Fe-Zn catalysts [18], and it has been proposed that water, a primary product in the FTS reaction can inhibit paraffin formation [21]. Since CO_2 addition increases the reverse rate of the WGS reaction, it increases H_2O concentration in the vicinity of the catalyst, which in turn could cause an increase in the olefin content and lead to an increase in the α-olefin/*n*-paraffin ratio, in our case. Shown in Figure 9 are the individual formation rates for C_5 and C_{11} olefins and paraffins at 543 K. The pentene formation rate increases with the addition of CO_2 to synthesis gas, while that for pentane is almost unchanged, which indicates that the increase in the α-olefin/*n*-paraffin ratio is because of an increase in the olefin content rather than a decrease in the paraffin content. At higher carbon numbers (C_{11}), these effects are very small. Since from Figure 5b, the overall hydrocarbon synthesis rate is unaffected by CO_2 addition, the increase in olefin rate and the decrease in paraffin rate is due to the decreased surface hydrogen availability with increasing CO_2 pressure and increasing the probability of chain termination to an olefin rather than a paraffin. However, this is true mainly for low molecular weight hydrocarbons as observed from unchanged olefin and paraffin rates for C_{11} with CO_2 addition (Figure 9).

Conclusions

Promoters such as Cu and K_2CO_3 when added to Fe-based FTS catalysts, enhance the formation of CO_2. While Cu is the primary ingredient of the commercial low temperature WGS catalysts, its role on Fe catalysts is in enhancing the primary formation of CO_2 *via* CO oxidation. At high temperatures, catalysts reach a limiting CO_2 selectivity, which is determined by the WGS reaction equilibrium. Addition of CO_2 to syngas serves to increase the reverse rate of WGS reaction and hence can increase hydrocarbon productivity. However, it does not appear to promote FT rates or affect the forward step of the WGS. CO_2 addition also decreases the net surface hydrogen concentration and produces more water, which causes a paraffin inhibition effect leading to higher olefin content. From our results it appears that the recycle of CO_2 formed during FTS can be used as a tool to improve the carbon efficiency of Fe catalysts, which in turn adds to their advantage of being cheaper and more flexible condition-wise than Co catalysts. (Observations from isotopic studies to be added here).

Acknowledgement

The authors would like to acknowledge the financial support provided by the U.S. Department of Energy (# DE-FC26-98FT40308) for this work.

References

1. F. Fischer and H. Tropsch, *Brennstoff-Chem.* 7 (1926) 97.
2. Anderson, R.B., The Fischer-Tropsch Synthesis, Academic Press, Orlando,FL, 1984.
3. Dry, M.E. The Fisher-Tropsch Synthesis, in *Catalysis-Science and Technology*, Vol. 1, p. 160, J. R. Anderson and M. Boudart eds., Springer Verlag, New York, 1981.
4. H. H. Storch, N. Golumbic and R. B. Anderson, *The Fischer-Tropsch and Related Syntheses*, Wiley, New York, 1951.
5. Vannice, M.A., *in* "Catalysis Science and Technology" (J.R. Anderson and M. Boudart eds.), p. 139. Springer-Verlag, Berlin, 1982; Vannice, M.A., *Catal. Rev. Sci. Eng.*, 3 (1976) 153.
6. Li, S., Li, A., Krishnamoorthy, S., and Iglesia, E., *submitted to Catal. Lett.*
7. Li, S., Krishnamoorthy, S., Li, A., Meitzner, G. D., and Iglesia, E., *submitted to J. Catal*.
8. Jin, Y. M., and Datye, A. K, *J. Catal.,* 196 (1) (2000) 8.
9. Newsome, D., *Catal. Rev. Sci. Eng*., 21 (2) (1980) 275.
10. Grenoble, D.C., Estadt, M.M., and Ollis, D.F., *J. Catal*., 67 (1981) 90.
11. Rethwisch, D.G., and Dumesic, J.A., *J. Catal*., 101 (1986) 35.
12. Lox, E.S., and Froment, G.F., *Ind. Eng. Chem. Res*., 32 (1993) 71.
13. Rao, K.R.P.M., Huggins, F.E., Mahajan, V., Huffman, G.P., Rao, V.U.S., Bhatt, B.L., Bukur, D.B., Davis, B.H., and O'Brien, R.J., *Top. Catal*., 2 (1995) 71.
14. Van der Laan, G.P., and Beenackers, A.A.C.M., *Appl. Catal. A*, 193 (2000) 39.
15. Li., S., Meitzner, G. D., and Iglesia, E., *J. Phys. Chem. B in press*.
16. Davis, B.H., Xu, L., and Bao, S., Natural Gas Conversion IV, *Stud. Surf. Sci. Cat.,* 107 (1997) 175.
17. Xu, L., Bao, S., Houpt, D.J., Lambert, S.H., and Davis, B.H., *Catal. Today*, 36 (1997) 347.
18. Soled, S.L., Iglesia, E., Miseo, S., DeRites, B.A., and Fiato, R.A., *Top. Catal*., 2 (1995) 193.
19. Utaka, T., Sekizawa, K., and Eguchi, K., *Appl. Catal. A*, 194-195 (2000) 21.
20. Bell, A. T., *Catal. Rev. Sci. Eng.*, 23 (1-2) (1981) 203.
21. Satterfield, C.N., and Stenger, H.G., *Ind. Eng. Chem. Proc. Des.*, 23 (1984) 26.

Figure 1. CO_2 selectivity as a function of CO conversion on the different Fe-Zn catalysts at (a) 508 K, 2.14 MPa, $H_2/CO=2$, and (b) 543 K, 0.5 MPa, $H_2/CO=2$. (▲): Fe-Zn, (◆): Fe-Zn-Cu_1, and (■): Fe-Zn-K_2, (●): Fe-Zn-K-Cu.

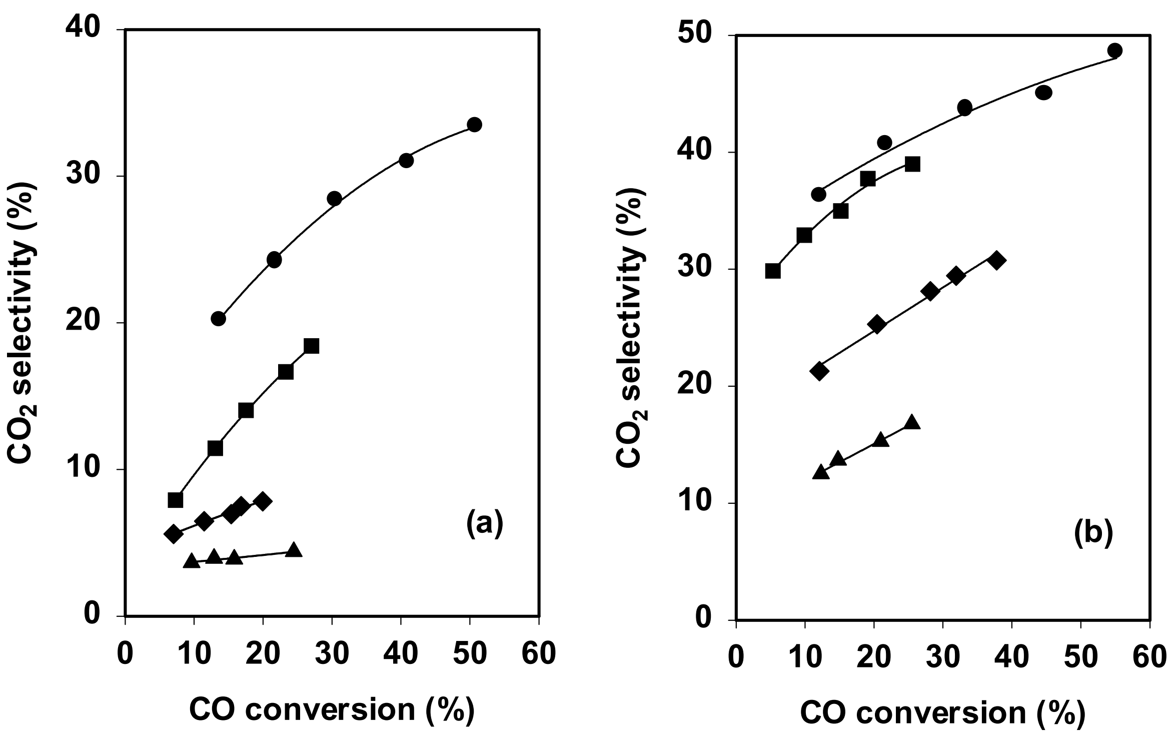

Figure 2. CO_2 selectivity (●) and Total oxygenates* (■) selectivity as a function of CO conversion on the Fe-Zn-K-Cu catalyst and 508 K, 2.14 MPa, $H_2/CO=2$.

(* - Alcohols, Aldehydes, Ketones and Acids)

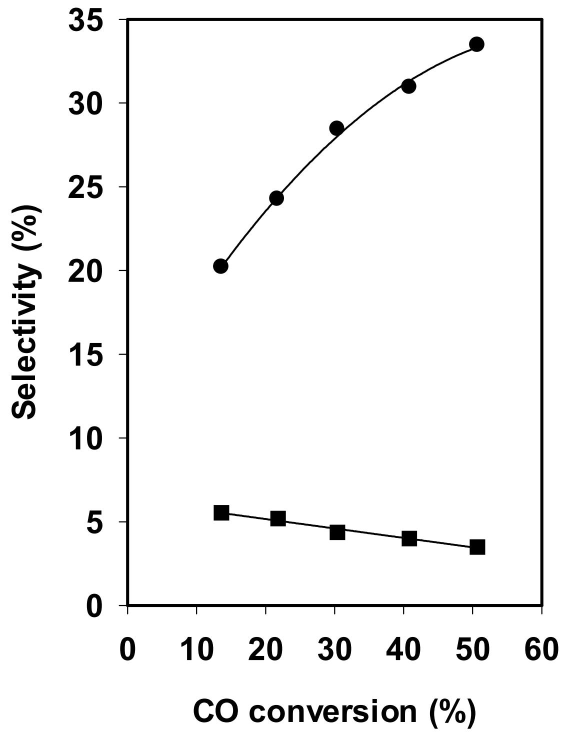

Figure 3. The extent of WGS reaction from equilibrium (η) as a function of the amount of CO_2 added for the Fe-Zn-K-Cu catalyst at (a) 508 K, 2.14 MPa, H_2/CO=2, and (b) 543 K and 0.5 MPa, H_2/CO=2.

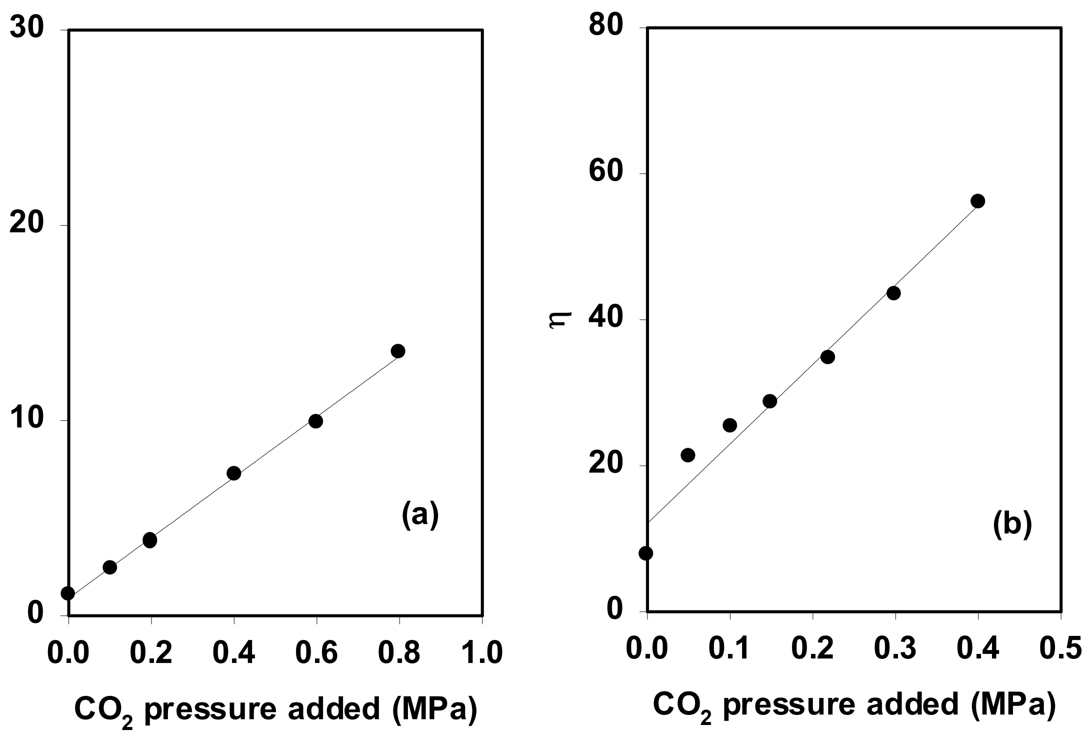

Figure 4. CO conversion (■), and syngas ($CO+H_2$) conversion (●) as a function of the amount of CO_2 added on the Fe-Zn-K-Cu catalyst at (a) 508 K, 2.14 MPa, $H_2/CO=2$, and (b) 543 K and 0.5 MPa, $H_2/CO=2$.

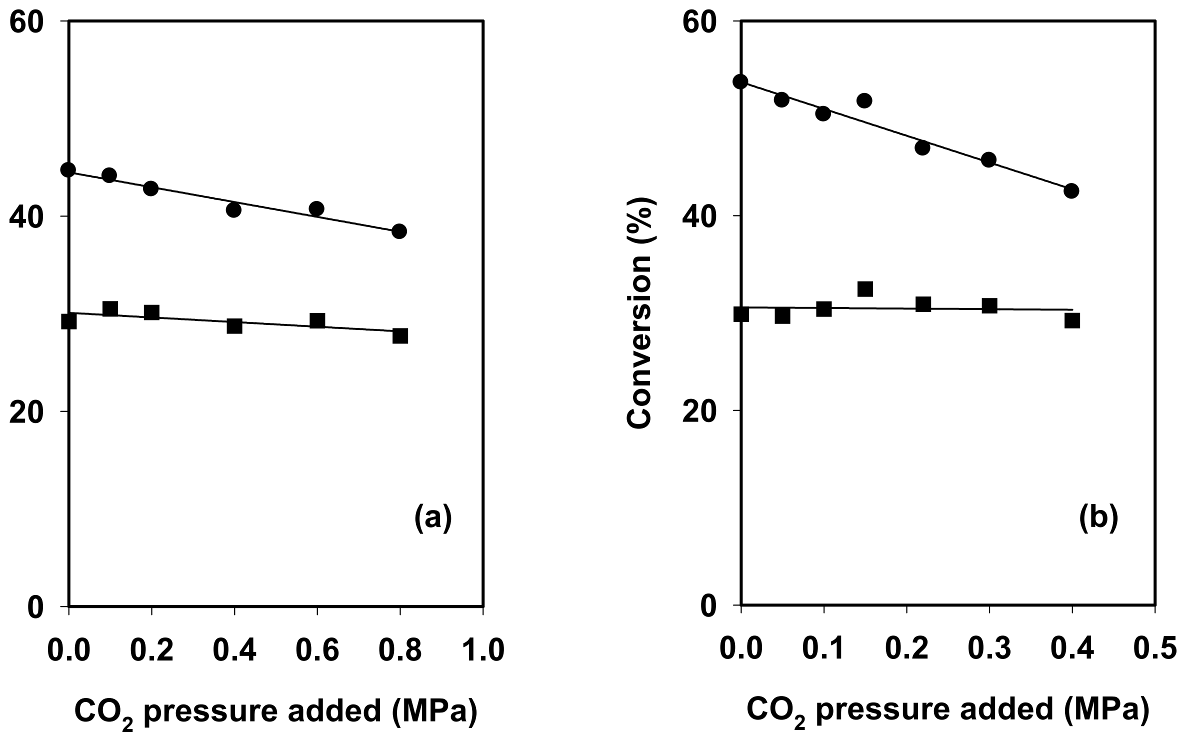

Figure 5. CO conversion rate (●), hydrocarbon formation rate (■) and CO_2 formation rate (▲), as a function of the amount of CO_2 added on the Fe-Zn-K-Cu catalyst at (a) 508 K, 2.14 MPa, $H_2/CO=2$, and (b) 543 K and 0.5 MPa, $H_2/CO=2$.

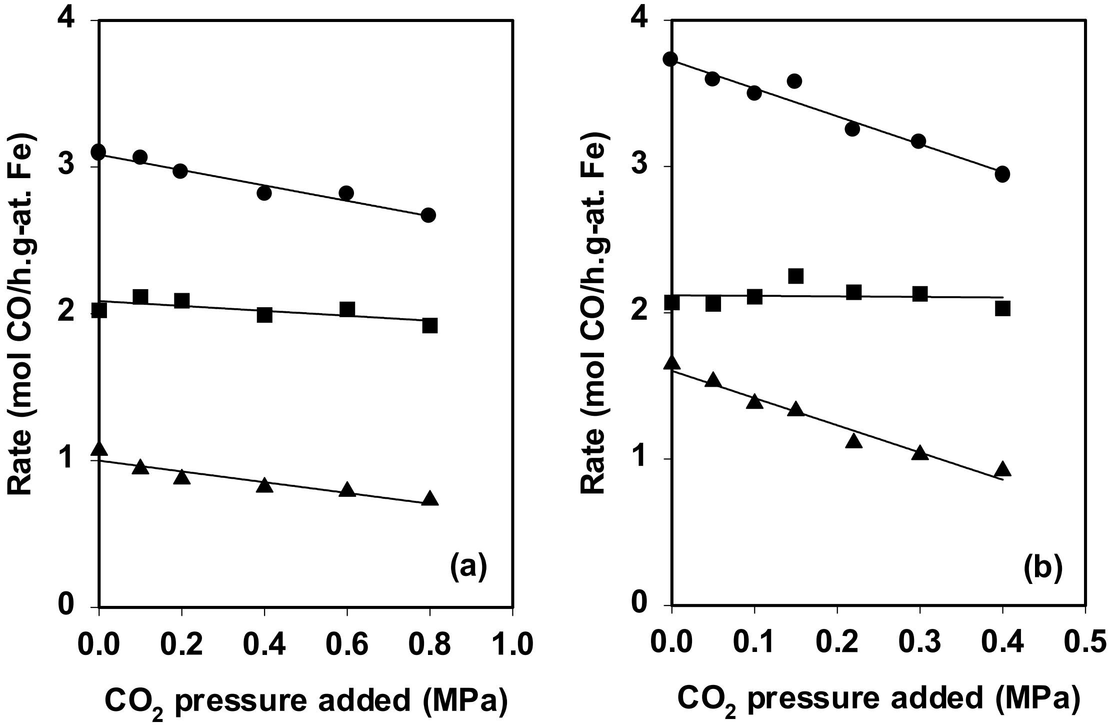

Figure 6. CO_2 forward rate (●), and CO_2 formation rate (■) as a function of the amount of CO_2 added on the Fe-Zn-K-Cu catalyst at 543 K and 0.5 MPa, $H_2/CO=2$.

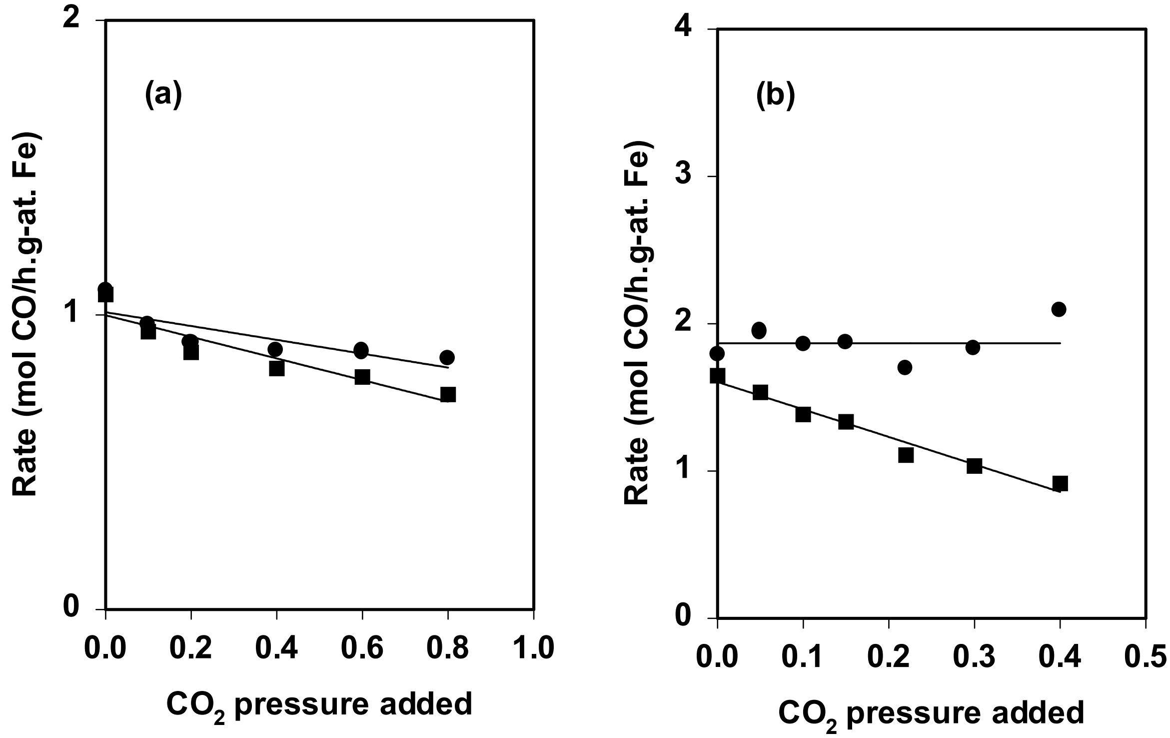

Figure 7. Product selectivities as a function of the amount of CO_2 added on the Fe-Zn-K-Cu catalyst at (a) 508 K, 2.14 MPa, H_2/CO=2, (b) 543 K and 0.5 MPa, H_2/CO=2; (●): C_{5+}, (■): CO_2 and (▲): CH_4.

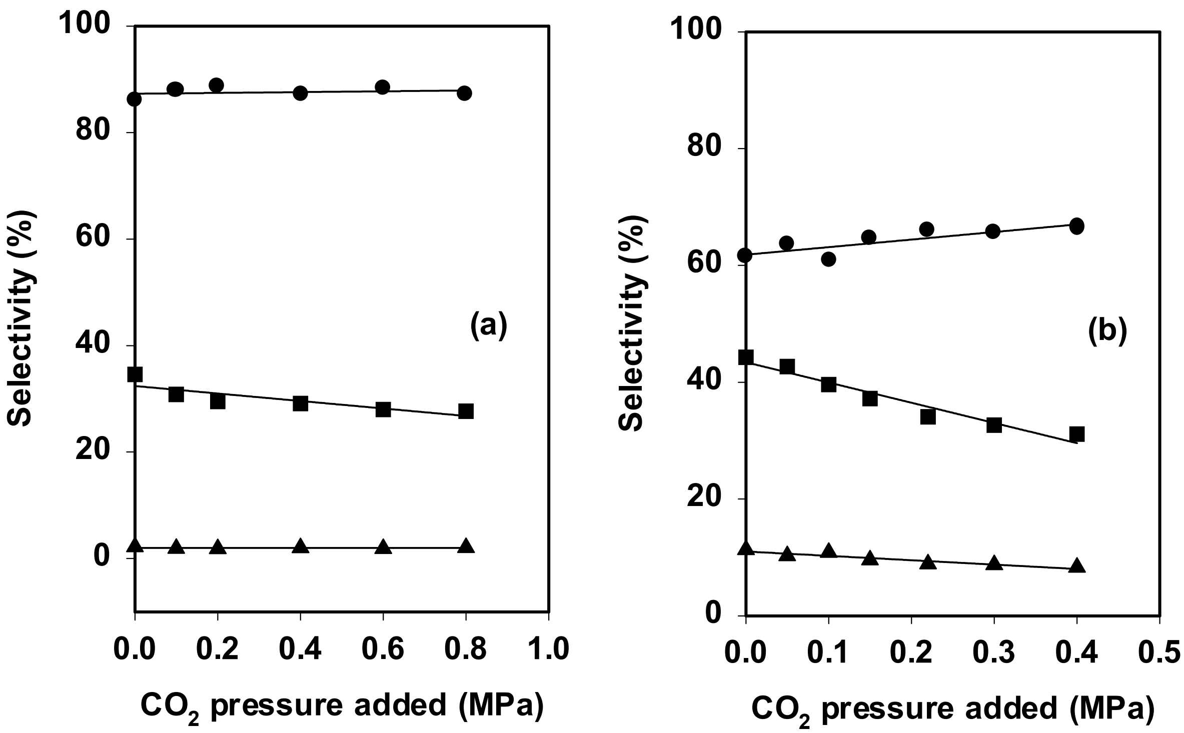

Figure 8. α-Olefin/n-paraffin ratio for different hydrocarbons as a function of the CO_2 pressure added on the Fe-Zn-K-Cu catalyst at (a) 508 K, 2.14 MPa, and (b) 543 K and 0.5 MPa, $H_2/CO=2$; (●): C_3H_6/C_3H_8, (■): 1-C_5H_{10}/n-C_5H_{12}, (▲): 1-$C_{11}H_{22}$/n-$C_{11}H_{24}$.

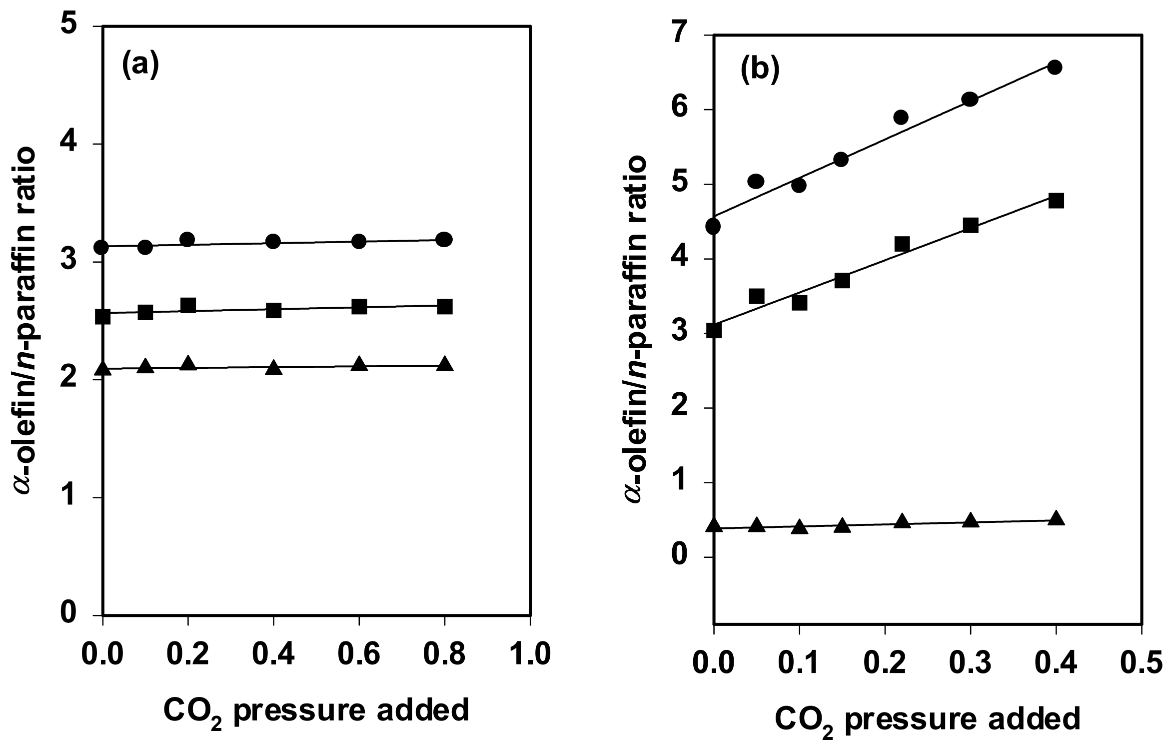

Figure 9. *1*-C_5H_{10} (○), *n*-C_5H_{12} (●), *1*-$C_{11}H_{22}$, (□) and *n*-$C_{11}H_{24}$ (■) formation rates as a function of the amount of CO_2 added on the Fe-Zn-K-Cu catalyst at 543 K and 0.5 MPa, H_2/CO=2.

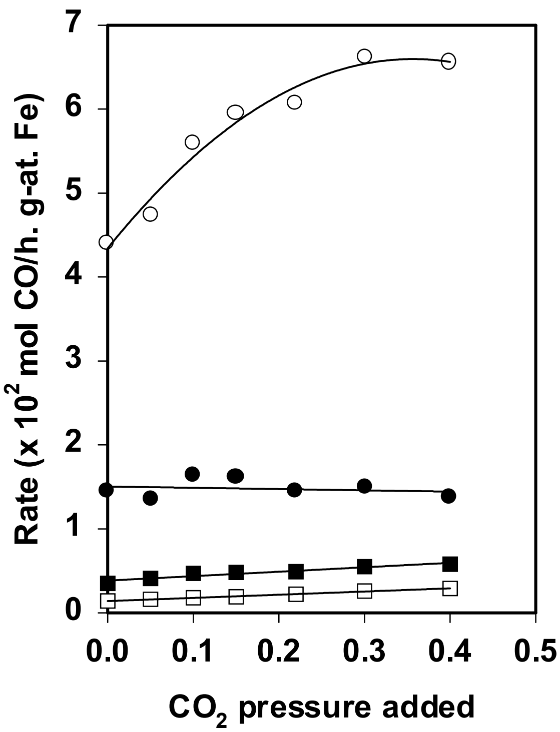

5.2 $^{13}CO_2$ addition studies on a Fe-Zn-Cu-K catalyst

$^{13}CO_2$ addition studies were initiated on a Fe-Zn-K-Cu (Zn/Fe=0.1, K/Fe=0.04, Cu/Fe=0.01) catalyst in order to determine the extent of participation of CO_2 in chain initiation and growth. These experiments will be conducted at conditions far away from equilibrium (i.e., 508 K and 0.8 MPa), and are being conducted in order to probe the extent of participation of CO_2 in chain initiation and growth mechanisms during CO hydrogenation.

Prior to these experiments, the sampling system at the outlet of the reactor system was modified. The vessel collecting liquids beyond the GC was placed under dry ice in order to separate the light gases from the rest of the components. 1ml of isopropanol was injected into this vessel via an injection port to dissolve the trapped components and form a homogeneous mixture. Both the gas as well as the liquid samples from this isolated vessel will be injected into a GC-MS to determine the ^{13}C fraction in the products. Simultaneously, a sample containing the effluent stream that enters the vessel will also be injected into this GC-MS to determine the 13C content in CO, CO_2 and the lower hydrocarbons (C_1-C_4). This type of sample collection procedure would lead to a higher sensitivity for ^{13}C analysis of intermediate hydrocarbon products.

II. FISCHER-TROPSCH SYNTHESIS ON COBALT CATALYSTS

1. Transient experiments with Co/SiO_2 catalysts

During the current period, switching experiments were performed at different space velocities on a 21.9% Co/SiO_2 catalyst, previously prepared [26], to estimate the carbon coverage at those conditions. The method used slightly differs from the one presented in the last report [27] by the fact that it takes into account the presence of a more active species of adsorbed carbon (carbon α) and a less active one (carbon β) and can evaluate the amount of only reactive carbon on the catalytic surface. The presence of carbon α and carbon β has been presented in the literature for iron based [28,29], and ruthenium based catalysts [30,31,32]. All the experiments hereby presented were performed switching from a mixture of syngas in argon ($H_2/CO/Ar$ = 62/31/7) to pure hydrogen. The switches were actuated at FT conditions and after reaching steady state, at constant pressure (0.5 MPa) and temperature (453 K) and at different space velocities. Argon was used as internal hydrodynamic standard, to estimate the time constant τ from fitting its recorded decay to the equation:

$$F(t) = F_1 + (F_2 - F_1)\cdot\left(1 - e^{-\frac{t-t_0}{\tau}}\right) \tag{II.1}$$

where t_0 is the time at which the transient begins, $F(t)$ (mol/s·g) is the flow rate at the time t (min), F_1 (mol/s·g) is the signal before the switch and F_2 (mol/s·g) the flow rate at the end of the transient. The model (II.1), derived by applying mass balances to a cascade of a continuous stirred reactor and a plug flow reactor, with no reaction, represents well the hydro dynamics of the system.

The flow rates were calculated for each component (CO, H_2, Ar, CH_4) according to the following equation:

$$F_i(t) = \left(\frac{F_i^0}{I_i^0}\right)\left(\frac{P_0}{P(t)}\right)\cdot I_i(t) \tag{II.2}$$

where, F^{i0} and I^{i0} are the flow rate (mol/s·g) and the intensity recorded n the MS (amps) of the component i, respectively, before the switch, P_0 (torr) is the pressure in the MS chamber before the switch and $P(t)$ and $I_i(t)$ are the pressure in the chamber and the intensity of the signal for the component i as recorded by the MS during the transient. Eq. (II.2) was derived considering that the flow of gas going to the MS may vary during the transient.

In Figure II.1 a typical experiment is reported, performed at 453 K, 0.5 MPa and with a bed residence time of 0.6 s. At these conditions the CO conversion was estimated from a gas chromatographic analysis to be 3.1%, the methane selectivity being 6.1%.

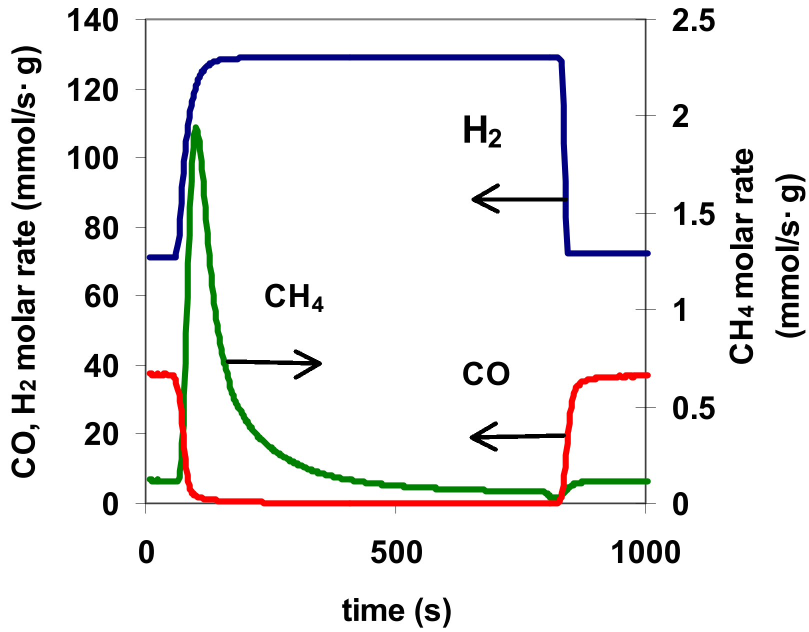

Figure II.1 - Switch from syngas to H_2 (P = 0.5 MPa, T = 453 K, τ = 0.6 s)

For the same experiment, Figure II.2 reports the decay of the argon flux, detected by the mass spectrometer, after the switch to hydrogen.

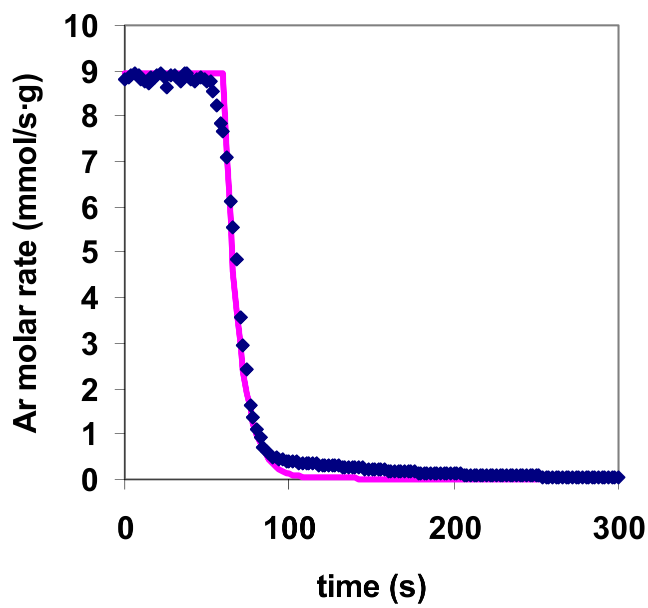

Figure II.2 - Switch from syngas to H_2 (P = 0.5 MPa, T = 453 K, τ = 0.6 s) - Ar decay. Dotted line = experimental points, solid line = flow calculated as from Eq. (II.2)

In Figure II.2 a fit of Eq. (II.1) to the experimental points is shown. The time constant τ, estimated by the fit, is 9 s.

To deconvolute the peak of methane, recorded during the transient, into two curves, to be attributed to hydrogenation of carbon α and carbon β, the descendant of the CH_4 flow rate was normalized and plotted in a logarithmic way versus time, as in Figure II.3.

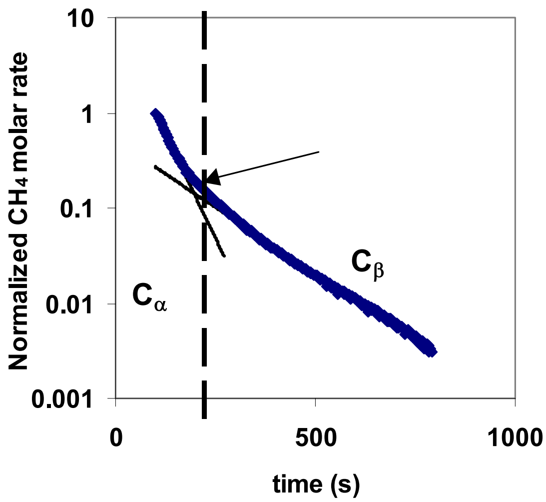

Figure II.3 - Switch from syngas to H_2 (P = 0.5 MPa, T = 453 K, τ = 0.6 s) - CH_4 normalized flow rate

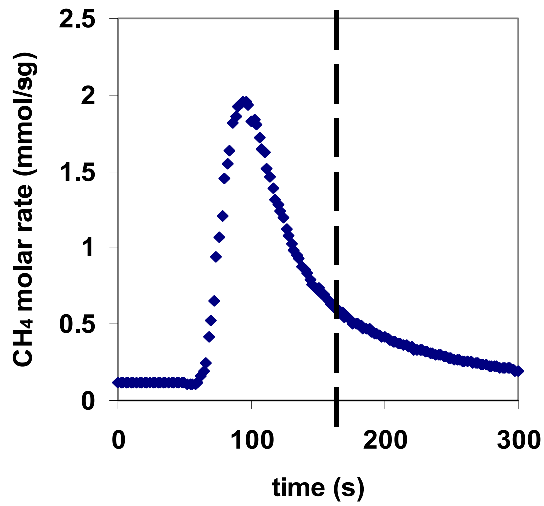

Figure II.4 - Switch from syngas to H_2 (P = 0.5 MPa, T = 453 K, τ = 0.6 s) - CH_4 flow rate

The two different slopes of the curve, evident in Figure II.3, were attributed to carbon α and carbon β, as shown in the picture. Therefore the integration of the methane peak was stopped at the time corresponding to the change in slope (Figure II.4), in order to consider the titration of the more active carbon (carbon α) only. The above described method was applied to a series of experiments collected a 0.5 MPa and 543 K, at different space velocities (from about 51 to 149 min^{-1}). The results are presented in Table II.1

Table II.1 - Experiments at P = 0.5 MPa, T = 453 K

SV (min^{-1})	Contact time (s)	CO conversion (%)	CH_4 selectivity (%)	Olefin selectivity	Rate (h^{-1})	p_{H2O} (atm)	θ_C (%)
149.2	0.40	2.5	6.0	0.14	18.74	0.02	8.8
101.4	0.59	4.7	4.8	0.1	22.87	0.04	11.6
76.2	0.79	5.9	3.8	0.09	23.04	0.05	11.7
51.2	1.17	9.4	3.7	0.08	24.62	0.08	12.1

On increasing CO conversion, (by decreasing space velocity) methane and olefin selectivity decreased, as expected. The increase in conversion and thus the increase in the average partial pressure of water on the reactor, led to a small increase in the rate of CO consumption and of the carbon coverage. The increase of reaction rate with water partial pressure and with the carbon coverage, could be explained by invoking a positive effect of water on the formation on the catalyst surface of active carbonaceous species, but the range of values of water partial pressure investigated is, though, rather small and can be misleading and not significant. Indeed the injection of water in the syngas downstream the reactor didn't enhance the catalyst activity as in previous experiments [19]. The absence of a beneficial effect of water on activity can be due to contaminants in the added water, or in the reactor. Also this behavior can come from the fact that the catalyst used has too large pores: it has been reported previously that Co/SiO_2 catalysts with large pores do not show a positive water effect, whereas those with small pores do [33].

For this reason further experiments on a Co/TiO_2 catalyst are at present being performed on a new catalyst: every TiO_2 supported catalyst proved in fact to show water effect on activity and selectivity [33].

III. APPENDIX

1. References

1. M. E. Dry, The Fisher-Tropsch Synthesis, in *Catalysis-Science and Technology*, Vol. 1, p. 160, J. R. Anderson and M. Boudart eds., Springer Verlag, New York, 1981.
2. F. Fischer and H. Tropsch, *Brennstoff-Chem.* 7 (1926) 97.
3. R. B. Anderson, in *Catalysis* Vol. 4, p. 29, P. H. Emmett eds., Van Nostrand-Reinhold, New York, 1956.
4. H. H. Storch, N. Golumbic and R. B. Anderson, *The Fischer-Tropsch and Related Syntheses*, Wiley, New York, 1951; R. B. Anderson, *The Fischer-Tropsch Synthesis*, Wiley, New York, 1984.
5. H. Kolbel and M. Ralek, *Catal. Rev.-Sci. Eng.* 21 (1980) 225.
6. J. W. Niemantsverdriet and A. M. van der Kraan, *J. Catal.* 72 (1981) 385.
7. J. A. Amelse, J. B. Butt and L. J. Schwartz, *J. Phys. Chem.* 82 (1978) 558.
8. G. B. Raupp and W. N. Delgass, *J. Catal.* 58 (1979) 348.
9. R. Dictor and A. T. Bell, *J. Catal.* 97 (1986) 121.
10. J. P. Reymond, P. Meriaudeau and S. J. Teichner, *J. Catal.* 75 (1982) 39.
11. C. S. Kuivila, P. C. Stair and J. B. Butt, *J. Catal.* 118 (1989) 299.
12. C. S. Huang, L. Xu and B. H. Davis, *Fuel Sci. Tech. Int.* 11 (1993) 639.
13. S. Soled, E. Iglesia and R. A. Fiato, *Catal. Lett.* 7 (1990) 271.
14. S. Soled, E. Iglesia, S. Miseo, B. A. DeRites and R. A. Fiato, *Topics in Catal.* 2 (1995) 193.
15. E. Iglesia, A research proposal submitted to the Division of Fossil Energy.
16. R. J. O'Brien, L. Xu. R. L. Spicer and B. H. Davis, *Energy and Fuels*, 10 (1996) 921.
17. D. B. Bukur, D. Mukesh, and S. A. Patel, *Ind. Eng. Chem. Res.*, 29, 194 (1990).
18. 1st Quarterly report, 1999. U.S. Department of Energy under contract # DE-FC26-98FT40308.
19. 2nd Quarterly report, 1999. U.S. Department of Energy under contract # DE-FC26-98FT40308.
20. 3rd Quarterly report, 1999. U.S. Department of Energy under contract # DE-FC26-98FT40308.
21. 4th Quarterly report, 1999. U.S. Department of Energy under contract # DE-FC26-98FT40308.
22. 1st Quarterly report, 2000. U.S. Department of Energy under contract # DE-FC26-98FT40308.
23. 2nd Quarterly report, 2000. U.S. Department of Energy under contract # DE-FC26-98FT40308.
24. 3rd Quarterly report, 2000. U.S. Department of Energy under contract # DE-FC26-98FT40308.
25. 4th Quarterly report, 2000. U.S. Department of Energy under contract # DE-FC26-98FT40308.
26. 1st Quarterly report, 2001. U.S. Department of Energy under contract # DE-FC26-98FT40308.
27. 2nd Quarterly report, 2001. U.S. Department of Energy under contract # DE-FC26-98FT40308.
28. D. Bianchi, Borcar S., Teule-Gay F., and Bennet C. O., *J. Catal.* 82 (1983) 442.

29. D. Bianchi, Tau L. M., Borcar S., and Bennet C. O., *J. Catal.* 84 (1983) 358.
30. P. Winslow, and Bell A. T., *J. Catal,* 158 (1984) 86.
31. P. Winslow, and Bell A. T., *J. Catal,* 385 (1985) 94.
32. M. De Pontes, Yokomizo G. H., and Bell A. T., *J. Catal.* 104 (1987) 147.
33. Iglesia E., *Appl. Catal.* 161 (1997) 59.

Task 12. Reporting/Project Management

Three monthly and one quarterly reports have been completed.